

---

Theses and Dissertations

---

Spring 2016

# An automated method of generating NURBS meshes for patient-specific geometries

Moustafa Galal Ibrahim  
*University of Iowa*

Copyright 2016 Moustafa Ibrahim

This thesis is available at Iowa Research Online: <http://ir.uiowa.edu/etd/3109>

---

## Recommended Citation

Ibrahim, Moustafa Galal. "An automated method of generating NURBS meshes for patient-specific geometries." MS (Master of Science) thesis, University of Iowa, 2016.  
<http://ir.uiowa.edu/etd/3109>.

---

Follow this and additional works at: <http://ir.uiowa.edu/etd>

 Part of the [Biomedical Engineering and Bioengineering Commons](#)

AN AUTOMATED METHOD OF GENERATING NURBS MESHES FOR PATIENT-  
SPECIFIC GEOMETRIES

by

Moustafa Galal Ibrahim

A thesis submitted in partial fulfillment  
of the requirements for the Master of Science  
degree in Biomedical Engineering in the  
Graduate College of  
The University of Iowa

May 2016

Thesis Supervisor: Associate Professor Sarah Vigmostad

Copyright by  
MOUSTAFA GALAL IBRAHIM  
2016  
All Rights Reserved

Graduate College  
The University of Iowa  
Iowa City, Iowa

CERTIFICATE OF APPROVAL

---

MASTER'S THESIS

---

This is to certify that the Master's thesis of

Moustafa Galal Ibrahim

has been approved by the Examining Committee for  
the thesis requirement for the Master of Science degree  
in Biomedical Engineering at the May 2016 graduation.

Thesis Committee:

\_\_\_\_\_  
Sarah Vigmostad, Thesis Supervisor

\_\_\_\_\_  
Jia Lu

\_\_\_\_\_  
Nicole Grosland

\_\_\_\_\_  
H.S. Udaykumar

\_\_\_\_\_  
Edward Sander

I would like to dedicate this to my parents for never giving up on me, and insuring that I see my dreams come through.

*“To be or not to be...”*

William Shakespeare  
Hamlet

## ACKNOWLEDGEMENTS

I would like to acknowledge my family for sticking by my side this entire time. Also for not giving up on me even when I doubted myself. Without their constant support I would of never made it this far. I would like to take this opportunity to acknowledge and thank my advisor and mentor Dr. Sarah Vigmostad for guiding me through this journey.

Additionally, I would like to thank Aaron, Nirmal, Anas, Mahmoud, Oishik, Liza, Piyusha, Keshav, Seth, John, Pratik, Kayley, Jarred, Sid, Mike and Ehsan who made my time in the lab worthwhile.

## ABSTRACT

Cardiovascular disease is the number one reason for emergency room visits in the United States. Understanding the different pathologies of the cardiovascular system is crucial when trying to prescribe proper treatment or intervention. In order best understand these issues proper computer simulations would be necessary. Due to the fact that every patient is different. Being able to analysis and properly simulate each patients data individually to better understanding their specific case is necessary for patient specific interventions. In order to achieve such requirement we propose a new method of mesh generation to better map patient specific geometries. This new framework takes a set of points in a 3D space and generates a 2D NURBS mesh. Insuring a smooth and accurate representation of the patient specific geometry will allow for more specific incite to possible medical issues that may arise. This NURBS based mesh can be then used to run either finite element analysis, computational fluid dynamics, or even fluid solid interactions. Running these patient-specific valve simulations using isogementric modeling is what will allow us to have patient specific treatments and intervention.



## PUBLIC ABSTRACT

Cardiovascular disease is the number one reason for emergency room visits in the United States. Understanding the different pathologies of the cardiovascular system is crucial when trying to prescribe proper treatment or intervention. In order best understand these issues proper computer simulations would be necessary. Due to the fact that every patient is different. Being able to analysis and properly simulate each patients data individually to better understanding their specific case is necessary for patient specific interventions. In order to achieve such requirement we propose a new method of mesh generation to better map patient specific geometries. This new framework takes a set of points in a 3D space and generates a 2D NURBS mesh. Insuring a smooth and accurate representation of the patient specific geometry will allow for more specific incite to possible medical issues that may arise. This NURBS based mesh can be then used to run either finite element analysis, computational fluid dynamics, or even fluid solid interactions. Running these patient-specific valve simulations using isogementric modeling is what will allow us to have patient specific treatments and intervention.

## TABLE OF CONTENTS

LIST OF TABLES .....	ix
LIST OF FIGURES .....	x
CHAPTER 1: INTRODUCTION .....	- 1 -
1.1 Overview .....	- 1 -
1.2 Aim.....	- 1 -
CHAPTER 2: BACKGROUND .....	- 3 -
2.1 Valve Anatomy and Pathologies.....	- 3 -
2.1.1 Geometry of Mitral and Aortic Valves .....	- 4 -
2.1.2 Congenital Heart Defects and Disease.....	- 6 -
2.1.3 Treatment and Interventions.....	- 8 -
2.2 Finite Element Modeling.....	- 11 -
2.2.1 Finite Element Modeling.....	- 11 -
2.2.2 Computational Fluid Dynamic Modeling .....	- 11 -
2.2.3 Fluid Solid Interaction Modeling .....	- 12 -
2.2.4 Motivation .....	- 12 -
2.3 NURBS Background and Overview .....	- 13 -
2.3.1 B-Spline Basis Function.....	- 13 -
2.3.2 NURBS Curves and Surfaces.....	- 15 -
2.3.3 Motivation .....	- 18 -
CHAPTER 3: AUTOMATED NURBS MESH GENERATOR .....	- 19 -
3.1 Introduction.....	- 19 -
3.2 Main Framework.....	- 19 -
3.2.1 NURBS Basis Functions .....	- 22 -
3.2.2 Surface Smoothing.....	- 24 -
3.2.3 Moving Control Points.....	- 27 -
3.3 Steepest Descent Algorithm .....	- 29 -
3.3.1 Cost Function.....	- 31 -
3.3.2 Gradient.....	- 32 -
3.3.3 Golden Section Method .....	- 33 -
CHAPTER 4: RESULTS AND DISCUSSION.....	- 36 -
4.1 Introduction.....	- 36 -

4.2 Analytical Geometries .....	- 36 -
4.2.1 Cylinder .....	- 36 -
4.2.2 Cone .....	- 38 -
4.2.3 Sphere.....	- 40 -
4.3 Patient Specific Point clouds .....	- 43 -
4.3.1 Patient-Specific Mitral valve Point clouds.....	- 43 -
4.3.2 Patient-Specific Coronary Artery Point clouds .....	- 44 -
4.4 Future Work.....	- 46 -
4.5 Summary.....	- 46 -
REFERENCES.....	- 48 -

## LIST OF TABLES

TABLE 1: RMS VALUES FOR PERCENT ERROR FOR ALL THREE ANALYTICAL SHAPES.....	- 42 -
TABLE 2: PATIENT SPECIFIC CORONARY ARTERY POINT CLOUD SPECIFICATIONS. ....	- 44 -

## LIST OF FIGURES

FIGURE 1: SAGITTAL PLAN SEGMENTATION OF THE HEART EXPOSING THE LEFT AND RIGHT CAVITIES (LEFT), AXIAL PLAN SEGMENTATION OF THE HEART REVELING ALL FOUR HEART VALVES (RIGHT) .....	- 3 -
FIGURE 2: A VERTICAL DISSECTION OF THE MITRAL VALVE, HERE THE MITRAL VALVE LEAFLETS ARE ATTACHED TO THE INTERIOR OF THE LEFT VENTRICLE THROUGH THE CORD LIKE STRUCTURES CALLED CHORDEA TENDINEA- 5 -	- 5 -
FIGURE 3: AORTIC VALVE IN THE OPEN AND CLOSED POSITION.....	- 6 -
FIGURE 4: HEALTHY AORTIC VALVE (LEFT), A STENOTIC VALVE (RIGHT).....	- 6 -
FIGURE 5: HEALTHY MITRAL VALVE IN THE FULLY CLOSED POSITION (LEFT), MITRAL VALVE WITH PROLAPSE IN THE CLOSED POSITION (RIGHT).....	- 7 -
FIGURE 6: FUSED AORTIC VALVE.....	- 8 -
FIGURE 7: BI-LEAFLET HEART VALVE (LEFT), TRI-LEAFLET HEART VALVE (CENTER), AND BALL AND CAGE HEART VALVE (RIGHT) ....	- 10 -
FIGURE 8: BIOPROSTHETIC HEART VALVE, MADE USUALLY FROM PORCINE OR BOVINE TISSUE AND A MESH LIKE ANNULUS RING.....	- 10 -
FIGURE 9: B-SPLINE WITH FOUR CONTROL POINTS .....	- 13 -
FIGURE 10: BASIS FUNCTION TRIANGULAR DEPENDENCY EACH HIGHER ORDER BASIS FUNCTION IS DEPENDENT ON TWO BASIS FUNCTION OF THE ONE LESSER ORDER .....	- 15 -
FIGURE 11: 1D NURBS REPRESENTATION .....	- 16 -
FIGURE 12: OVERVIEW FLOW OF AUTOMATED NURBS GENERATOR.....	- 21 -
FIGURE 13: THE SELECTION OF THE CONTROL POINTS BEING SELECTED TO GENERATE INDIVIDUAL PATCHES .....	- 22 -
FIGURE 14: INITIAL GENERATION OF 1D NURBS CURVE BEFORE CONTROL POINTS ARE MOVED.....	- 23 -
FIGURE 15: 2D NURBS SURFACE GENERATED .....	- 24 -
FIGURE 16: SELECTING APPROPRIATE POINTS FOR INTERPOLATION BETWEEN THE LEADING POINT AND THE SEAM AND THE TRAILING POINT AND THE SEAM FOR A 1 D CASE .....	- 26 -
FIGURE 17: THE ADDITION OF TWO NEW POINT CLOUD POINTS CAN BE SEEN IN RED.....	- 27 -

FIGURE 18: INITIAL EVALUATION POINTS WHEN MARCHING A FULL KNOT SPACING.....	- 28 -
FIGURE 19: TEN EVALUATIONS ARE DONE PER LINE SEGMENT AND THE CLOSEST SURFACE POINT ARE DETECTED.....	- 29 -
FIGURE 20: FLOW CHART REPRESENTING ITERATIVE PROCESS OF THE STEEPEST DESCENT.....	- 30 -
FIGURE 21: GOLDEN SECTION SEARCH REPRESENTATION.....	- 35 -
FIGURE 22: GENERATED CYLINDRICAL POINT CLOUD THAT IS CENTERED ON THE Z-AXIS WITH A RADIUS OF 1 AND A HEIGHT OF 2.....	- 37 -
FIGURE 23: OPTIMIZED NURBS GENERATION OF CYLINDRICAL POINT CLOUD.....	- 38 -
FIGURE 24: GENERATED CONE POINT CLOUD .....	- 39 -
FIGURE 25: OPTIMIZED NURBS SURFACE GENERATED BY CONE POINT CLOUD.....	- 39 -
FIGURE 26: GENERATED SPHERICAL POINT CLOUD WITH A RADIUS 1....	- 40 -
FIGURE 27: OPTIMIZED NURBS SURFACE GENERATED FROM SPHERICAL POINT CLOUD .....	- 41 -
FIGURE 28: SCATTERED PLOT OF PERCENT ERROR BETWEEN NURBS GENERATED SURFACE AND ANALYTICAL SOLUTIONS FOR: SPHERE, CONE AND CYLINDER .....	- 42 -
FIGURE 29: OPTIMIZED NURBS SURFACE OF PATIENT 1 MITRAL VALVE FROM POINT CLOUD .....	- 43 -
FIGURE 30: OPTIMIZED NURBS SURFACE OF PATIENT 2 MITRAL VALVE FROM POINT CLOUD .....	- 44 -
FIGURE 31: OPTIMIZED NURBS SURFACE OF PATIENT 1 CORONARY ARTERY FROM POINT CLOUD .....	- 45 -
FIGURE 32: OPTIMIZED NURBS SURFACE OF PATIENT 2 CORONARY ARTERY FROM POINT CLOUD .....	- 45 -
FIGURE 33: OPTIMIZED NURBS SURFACE OF PATIENT 3 CORONARY ARTERY FROM POINT CLOUD .....	- 46 -

## CHAPTER 1: INTRODUCTION

### 1.1 Overview

Heart disease is the leading cause of death in the United States. According to the American Heart Association in 2012 about 1 in of 3 adults aged 18 and over reported being diagnosed at least cardiovascular disease [1]. Cardiovascular disease may be characterized by, but not limited to, thrombi formation, valvular stenosis, and genetic mutations [2]. Furthermore, there are various complications that may occur when treating cardiovascular disease. Some of the listed conditions can be further studied to help decrease any future complications in the clinical setting. Many studies on cardiovascular diseases are conducted by computer simulations [3]. For example, studying Abdominal Aortic Aneurysms (AAA), looking into the blood flow dynamics can give solid incite to possible rupture points and conditions [4].

There have been many studies showing the role of computational fluid dynamics (CFD) simulations in prescribing treatments of vascular pathologies [5]. However, there are a number of challenges involved when using computational simulations. One main challenge is maintaining an accurate representation of the geometry while minimizing the computational cost. Future clinical issues can be predicted when there is high coaptation between the generated mesh and the object surface [3].

### 1.2 Aim

Common types of generated mesh elements use triangular or quadrilateral algorithms. These methods may be advantageous when meshing geometries with straight

edges, representing straight edges with a series of segmented lines may seem trivial. However, when trying to mesh irregularly shaped biological tissue, such as heart valves, veins or arteries, it may not be an optimal method. The research work to be presented uses an automated method of a Non-Uniform Rational B-Spline (NURBS) mesh generation. The power of NURBS allows us to generate mesh elements using b-splines. This allows us to better represent irregular objects commonly seen in cardiovascular tissue. In this work, the process about generating a NURBS-based mesh from a point cloud is shown. The end-goal is to evaluate this method and its potential application to the cardiovascular system.



## CHAPTER 2: BACKGROUND

### 2.1 Valve Anatomy and Pathologies

The heart contains four valves which divide four spatial chambers: the mitral, tricuspid, aortic and pulmonary valve. The mitral valve, also known as the bicuspid valve, separates the left atrium (LA) and the left ventricle (LV). The tricuspid valve separates the right ventricle (RV) and the right atrium (RA). The pulmonary valve is attached to the RV. Finally, the aortic valve is located between the LV and the aorta. The main job for any valve in the circulatory system is to establish a unidirectional flow. Due to the very thin and flexible tissue, these valves undergo quick deformations during their opening and closing phases.

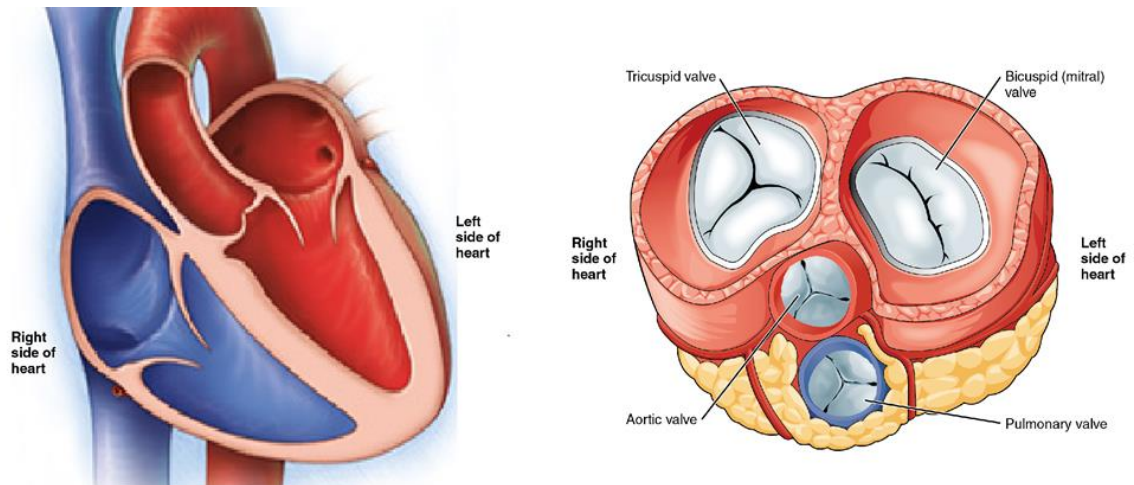


Figure 1: Sagittal plan segmentation of the heart exposing the left and right cavities (left), axial plan segmentation of the heart revealing all four heart valves (right).

The cardiac cycle consist of two phases, systole and diastole. The systolic phase is when the left and right ventricles contract. During this phase, blood flows from the RV out to the lungs through the pulmonary valve. Simultaneously, blood flows out of the LV past

the aortic valve, to disperse blood throughout the body. This is also known as the ejection phase. During this contraction, the aortic and pulmonary valves are forced open due to an induced pressure difference [6]. At the end of the ejection phase, the aortic and pulmonary valves close, and the bilateral atrial compartments contract. This phase is known as diastole or the filling phase, due to the refilling of the LV and RV compartments.

In order for the circulatory process to work, the arteries and valves must be completely healthy and functioning normally. Some pathologies may be induced due to poor diet or unhealthy life styles. Also, due to how often these valves open and close, they can be prone to mechanical damage. However, valves may also be damaged due to genetic anomalies, causing there to be a defect at birth. For example, the aortic valve normally has three leaflets, however some infants are born with two leaflets fused together, known as bicuspid aortic valves [7]. Atherosclerotic lesions can also lead to abnormal blood flow. There are many other complex cardiovascular conditions, and therefore, it may be difficult to determine an optimal medical treatment among a general patient population. Therefore, studying each patient case individually is very crucial.

### 2.1.1 Geometry of Mitral and Aortic Valves

The mitral valve is a bicuspid valve that separates the LV and LA. The mitral valve consists of two leaflets (posterior and anterior), an annulus, and the chordae tendineae. The thickness of the two leaflets in the mid-section usually measure to be approximately  $0.97 \pm 3$  mm [8]. This thin membrane allows for quick and smooth deformation. Under normal conditions, there is complete coaptation, which assures that, while in the fully closed position, there will not be any blood flowing back into the LA[9]. The mitral valve operates to guide blood flow to be unidirectional. Encompassing these two leaflets is the annulus,

which is a circular band that provides an attachment point for the leaflets. This band is made out of collagen and elastin fibers to allow it to easily deform throughout the cardiac cycle. On average, the annulus can stretch between 5-10mm [8]. The elastic fibers that are attached to the backside of these leaflets are known as the chordae tendineae. The chordae tendineae are string-like tissues that prevent the leaflets from relapsing. The chordae tendineae is attached to the papillary muscles in the LV, which aid to assure the leaflets are not inverted into the LA when fully closed [10].

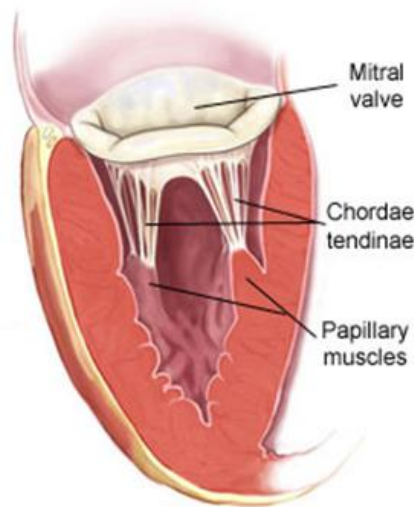


Figure 2: A vertical dissection of the mitral valve, here the mitral valve leaflets are attached to the interior of the left ventricle through the cord like structures called chordea tendinea.

The aortic valves is a tricuspid valve which ensures unidirectional blood flow out of the LV and into the systemic circulation. This valve consists of three leaflets. Similarly to the mitral valve, the aortic valves also contains an annulus that surrounds the leaflets. The aortic valve goes through various pressure changes which increases the risk to mechanical damage [11].

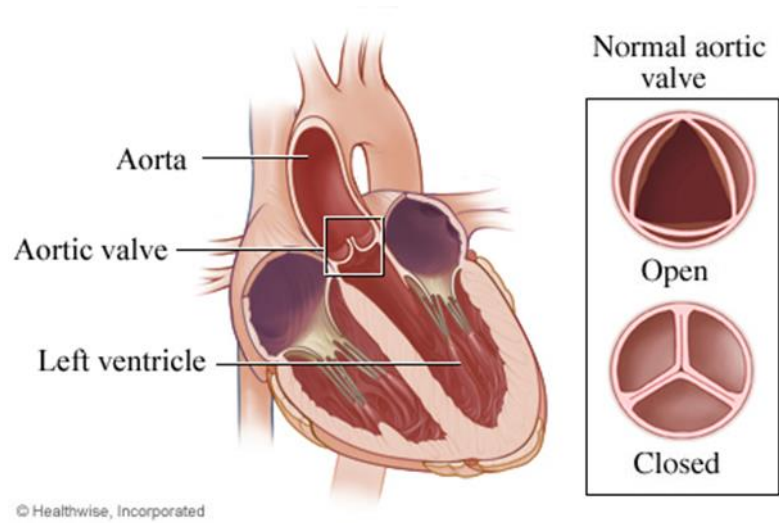


Figure 3: Aortic Valve in the open and closed position.

### 2.1.2 Congenital Heart Defects and Disease

There are many possible different types of valve defects and diseases. Some diseases may develop over time, while others may occur at birth. Stenotic tissue, for example, is a condition which develops over time. A very common place for this type of tissue to form is on the valve leaflet which causes stiffness of the tissues [12]. When the leaflets reach a particular level of stenosis, they can no longer completely close.

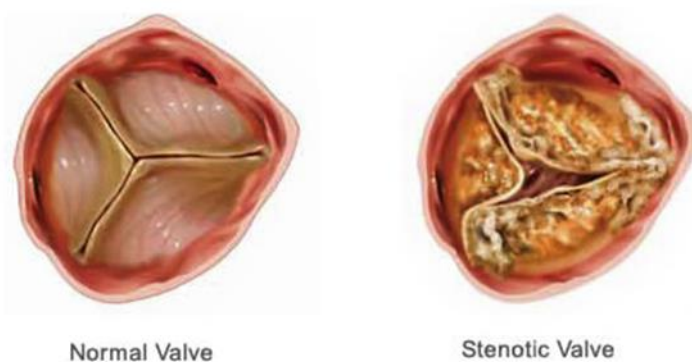


Figure 4: Healthy aortic valve (left), a stenotic valve (right).

One of the most common valvular conditions is regurgitation. Regurgitation, or “backflow”, is when blood starts seeping through a gap in the valve. This may prevent the blood from moving forward in the cardiac cycle. Regurgitation may be induced by a stenotic valve, and may also manifest to thrombus formation [12].

Coaptation of the leaflets are vital in order to prevent regurgitation [13]. Coaptation is the overlapping tissue of the leaflets when they come together in the closed position. However a mismatch in coaptation may sometimes occur leading again to some amount of regurgitation.

In mitral valve the weakness of the chorda tenednea can also cause a loss of structural integrity which then may lead to the leaflets not closing properly. This process of the leaflets ‘flopping’ or not closing properly is also known as mitral valve prolapse. An oversized leaflet can also cause there to be prolapses.

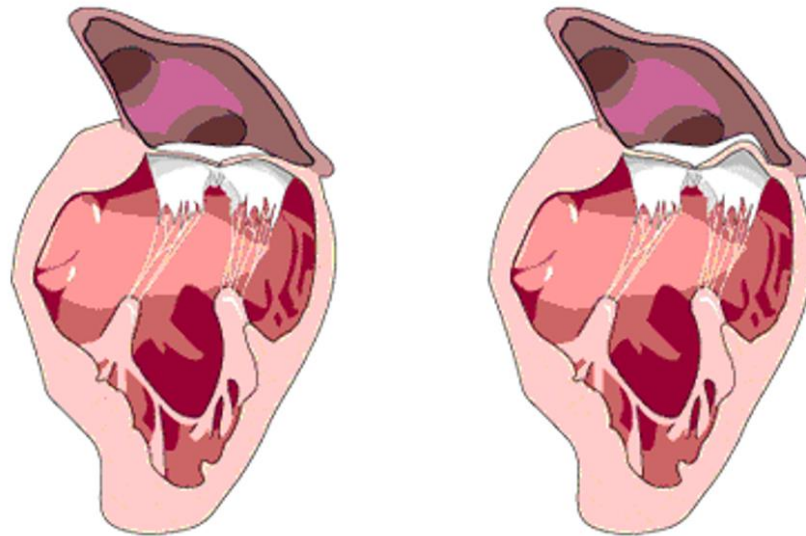


Figure 5: Healthy Mitral valve in the fully closed position (Left), Mitral valve with prolapse in the closed position (Right).

Another condition is when there are fused leaflets, typically seen as a congenital defect. This heart defect has been commonly observed in males, and affects the aortic valve. In most cases, the fusion is between the right and left cusps [14]. Those that demonstrate the congenital defect may also have a slight dilatation of the coronary arteries[13].

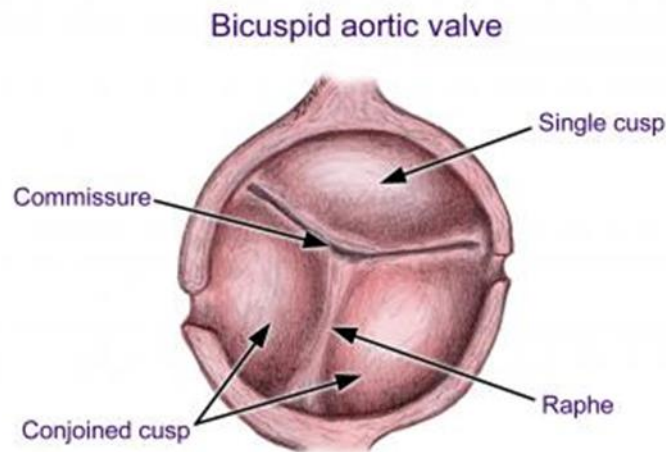


Figure 6: Fused aortic valve.

With such defect there has been a set of different interventions developed. These interventions are to try to insure that blood flow within the heart takes a normal path. Depending on the type of defect and which valve has been effected there are different potential approaches.

### 2.1.3 Treatment and Interventions

One potential intervention, or treatment, is having a heart valve replacement. Replacement heart valves can be either mechanical or bioprosthetic. In some cases, a surgical procedure can also be performed to manually repair the heart valve, thus avoiding valve replacement [15].

Repairing the mitral valve common procedure that has been developed. However not every mitral valve can be repaired. Mitral valve repairs have been shown to be advantageous in many ways, such as the success rates are much higher than valve replacements. Mitral valve repairs are also done minimally invasive which also reduces the chance of infections.

Currently, there are many existing designs of mechanical heart valves. The common designs include the ball and cage, tri-leaflet hinge or bi-leaflet hinge valves [16]. Each design has its advantages and disadvantages. Anticoagulants need to be prescribed to any patients undergoing a mechanical valve replacement procedure. This is because the replacement valve is detected as a foreign material being placed into the body, and the [17]. Furthermore, a molecular reaction may occur due to poor mismatch material compliance. Another complication is blood damage that can result from the high velocity blood flow through small gaps between leaflets or between the hinge and leaflet. When platelets are activated, there is an increased risk of thrombus formation. However, currently existing mechanical heart valves are extremely durable, and can last a patient's lifetime [17].



Figure 7: Bi-leaflet heart valve (left), Tri-leaflet heart valve (center), and ball and cage heart valve (right).

Another replacement method uses bioprosthetic heart valves. These valves are made from either bovine pericardial or porcine aortic valve tissue. The leaflet portion of these valves would be made of the biological tissue while the annulus is often made of a prosthetic support stent. This stent is designed to provide structural support and allow for tissue ingrowth. Bioprosthetic valves do not require the patient to take prescribed anticoagulants. However, these valves are much less durable, and often calcify, typically requiring replacement within 15 years of implantation [11]. Mitral valve repair is a very common form of treatment to treat cardiovascular disease. However, this intervention option is not ideal or even possible for all cases.



Figure 8: Bioprosthetic heart valve, made usually from porcine or bovine tissue and a mesh like annulus ring.



## 2.2 Computational Modeling

When trying to better understand how certain diseases effects the valves structural integrity or how the blood flow through these valves. The methods that are being used for such studies are finite element analysis (FEA), computational fluid dynamics (CFD), or fluid solid interaction (FSI). Each method delivers a set of insight, choosing what method to best use would depend on what is being studied.

### 2.2.1 Finite Element Modeling

With current standard FEA solvers the main focus is to look at the solid structure and see how it deform under different loads. Running a finite element simulation requires a either a shell element or a solid element. These element type are depending on a specific set of parameters there one can make a choice between a solid element and a shell element. Each element type has its advantages and setbacks with a shell element computational time is significantly lower however the depth of detail is also lost. In either case most common FEA programs and solvers can handle triangular and quadrilateral mesh elements. These are element types in which represent a surface or solid using a set number of triangular and quadrilateral for surface meshes and tetrahedral or brick elements for a solid mesh.

### 2.2.2 Computational Fluid Dynamic Modeling

The second type of simulations that are done would be computational fluid dynamics (CFD). With such analysis the main concern is the fluid flow. As in with FEM the mesh structure that is commonly used in most commercial CFD software have

triangular and quadrilateral for surface meshes and tetrahedral or brick elements for a solid mesh as there element types. CFD simulations are frequently used when studying blood flow with the cardiovascular system. When designing new implant the study of the fluid flow can and in some case is done experimentally however most commonly a CFD simulation are done. This allows for a more detailed study and understanding of how the blood dynamics would be.

### 2.2.3 Fluid Solid Interaction Modeling

Finally we come to a new method that has recently surfaced, fluid solid interaction (FSI). With FSI the solver looks at both solid structure and how it interacts with the fluid. These simulations are the most insightful yet also the most costly. The mesh structure for most FSI solvers are that of the FEM as well. With fluid structure interaction simulations the kinematics that are observed on not only one do to the initial boundary conditions however they are influenced by how the solid changes. For example when studying the fluid movement through a valve throughout a cardiac cycle, the valve deformation will affect the fluid moves [18].

### 2.2.4 Motivation

Studying physiological conditions on a computer simulation allow there to be large set of cases that be looked at. Understand with some level of detail what types of stress and deformations biological tissues undergo will help with diagnosing specific diseases. Being able to study and diagnose these diseases would lead into understanding and working on preventive care measure that might be taken.

## 2.3 NURBS Background and Overview

### 2.3.1 B-Spline Basis Function

The formulation of a Non-Uniform Rational B-Spline (NURBS) surface consists of a piece-wise function that is primarily B-Spline curves[19]. In order to formulate a NURBS surface a Knot vectors is needed. This also serves as the notation in parametric space (along the curve). A knot vector is a vector that is consist of a set of non-decreasing sequence of real numbers  $U = (u_0, u_1, u_2, u_3, \dots, u_m)$ ; Each value within this vector is referred to as a knot ( $u_i$ ). The number of knots in a knot vector is determined by the relationship in Equation 1 below. Where  $p$  is the power of the NURBS curve and  $k$  is the number of control points being used. In order to ensure the surface to be smooth and continues the only repeated values are the 'end caps' of the vector. Having repeating values at the 'end caps' also clamps down the first and last point. A representation of this can be seen in the Figure 8 below.

$$m = k + p + 1$$

*Equation 1*

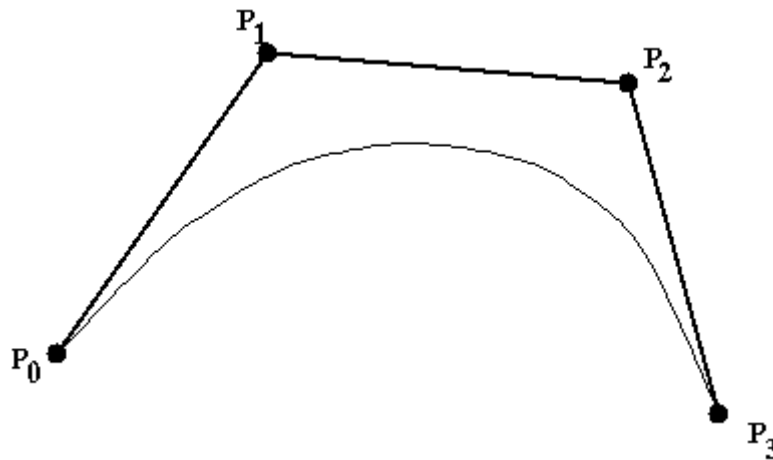


Figure 9: B-spline with four control points.

For practical purpose the example of the NURBS curve above being a 2<sup>nd</sup> order curve would have a knot vector similar to this  $U = (0,0,0,1,2,2,2)$ . The knot vectors are the basis of which the basis functions are generated.

The generation of the basis functions which when pieced together generated the NURBS curve or surface are generated using the knot values. The basis functions are a set of piecewise functions that are generated based on the desired degree (power). The basis function is generated in a way to smoothly fit through a set of points. Each basis function can be represented by  $N_{i,p}$ , where  $i$  is associated with the particular point and  $p$  represents the power. Because each basis function is associated with a specific knot points the notations becomes  $N_{i,p}(u)$ . This term is defined in the Equations below[19]:

$$N_{i,0}(u) = \begin{cases} 1 & u_i \leq u < u_{i+1} \\ 0 & \text{otherwise} \end{cases}$$

$$N_{i,p}(u) = \frac{u - U_i}{U_{i+p} - U_i} N_{i,p-1} + \frac{U_{i+p+1} - u}{U_{i+p+1} - U_{i+1}} N_{i+1,p-1} \quad \text{Equation 2}$$

For degrees greater than zero the basis function is simply an addition of two basis function with one lower degree. The basis functions have a triangular dependence this can be more visually seen in the Figure 9 below.

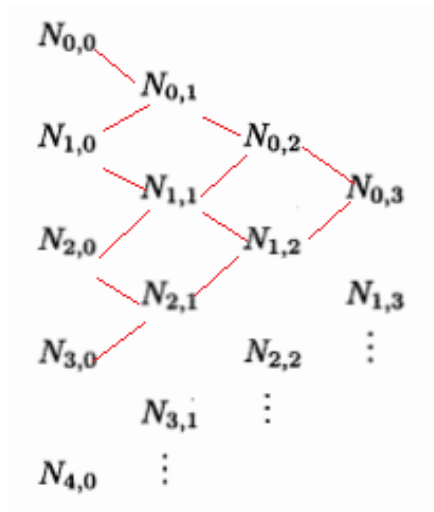


Figure 10: Basis function triangular dependency each higher order basis function is dependent on two basis function of the one lesser order.

### 2.3.2 NURBS Curves and Surfaces

In order to generate a NURBS curve, it is important to make sure there are points in Cartesian space that can depict the position and direction the NURBS needs to take. These points are referred to them as control points. The control points are used as guidance for the basis function when generating a NUBRS curve. The NURBS curve may or may not actually lie on a control point. The connectivity between the control points form what is known as the control point polygon, an example of this can be seen in the Figure 10 below.

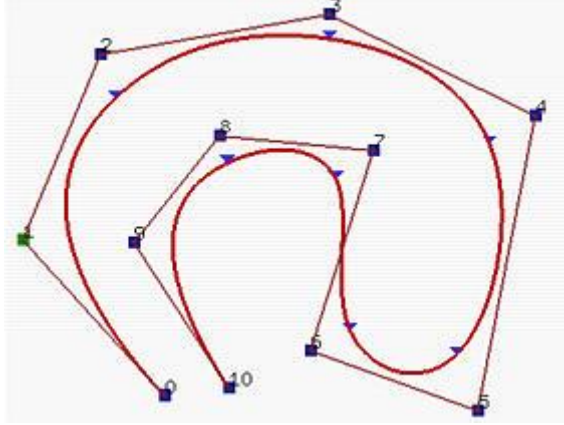


Figure 11: 1D NURBS representation.

In order to be able to completely generate a NURBS curve an addition parameter is needed which allow more control over the curve. The parameter that is needed are called weights. There should be a weight value for every control point. The weight value can be any real number greater than 0. Having higher weight value increases the control the associated control point has on the curve formation[20]. A NURBS curve with  $p$ -th degree is represent by  $C(u)$  in the Equation 3.

$$C(u) = \frac{\sum_{i=0}^n N_{i,p}(u) \cdot w_i \mathbf{P}_i}{\sum_{i=0}^n N_{i,p}(u) \cdot w_i} \quad \text{Equation 3}$$

$$w = (w_0, w_1, w_2, w_3, \dots, w_k)$$

Where  $w_i$  are the weight value,  $\mathbf{P}_i$  refers to the control point, and  $N_{i,p}(u)$  are the basis function. An alternative way to represent this NURBS curve can be seen in the Equation 4, below. Looking at the formulation below  $R_{i,p}(u)$ , represents the weighted shape functions for each control point.

$$R_{i,p}(u) = \frac{N_{i,p}(u) \cdot w_i}{\sum_{j=0}^n N_{j,p}(u) \cdot w_j} \quad \text{Equation 4}$$

$$C(u) = \sum_{i=0}^n R_{i,p}(u) \cdot P_i \quad \text{Equation 5}$$

Expanding this concept an additional parametric dimension allows us to generate NURBS surfaces. Similarly to the generation of the NURBS curve the NURBS surface has a  $u$ -direction and an additional direction  $v$ . A NURBS surface of degree  $p$  in the  $u$ -direction and  $q$  in the  $v$ -direction would have the following knot vectors:

$$U = (u_0, u_1, u_2, u_3, \dots, u_m) \quad m = k + p + 1$$

$$V = (v_0, v_1, v_2, v_3, \dots, v_n) \quad n = r + q + 1$$

Where here  $k$  is the number of control points in the  $u$ -direction and  $n$  is the number of control points in the  $v$ -direction. Expanding the NURBS representation to the second parametric dimension would have the following formulation as expressed by  $S(u,v)$  Equation 6, below.

$$S(u, v) = \frac{\sum_{i=0}^n \sum_{j=0}^m N_{i,p}(u) \cdot N_{j,q}(v) \cdot w_{i,j} \cdot P_{i,j}}{\sum_{i=0}^n \sum_{j=0}^m N_{i,p}(u) \cdot N_{j,q}(v) \cdot w_{i,j}} \quad \text{Equation 6}$$

$$w_{k,r} = \begin{bmatrix} w_{0,0} & w_{1,0} & w_{2,0} & \dots & w_{k,0} \\ w_{0,1} & & & & \\ w_{0,2} & & \ddots & & \vdots \\ \vdots & & & & \\ w_{0,r} & \dots & & & w_{k,r} \end{bmatrix}$$

In the NURBS surface representation above,  $S(u, v)$ ,  $P_{i,j}$  represents the control points in the  $u$ -direction and in the  $v$ -directions. Also as in the single dimension there is a specific weight value for each control point. A more effective way to represent a NURBS surface

can be seen in the Equation 7 and 8, below. Looking at the formulation below  $R_{i,j}(u,v)$ , represents the weighted shape functions for each control point

$$R_{i,j}(u, v) = \frac{N_{i,p}(u) \cdot N_{j,q}(v) \cdot w_{i,j}}{\sum_{k=0}^n \sum_{l=0}^m N_{k,p}(u) \cdot N_{l,q}(v) \cdot w_{k,l}} \quad \text{Equation 7}$$

$$S(u, v) = \sum_{i=0}^n \sum_{j=0}^m R_{i,j}(u, v) \cdot \mathbf{P}_{i,j} \quad \text{Equation 8}$$

### 2.3.3 Motivation

The use of NUBRS to properly represent the surface of biological tissues is superior to just using a typical triangular or quadrilateral mesh elements, due to the series of splines that can be generated to capture the surface compared to a series of lines. When working with an ordered point cloud the complications increase. Generating a smooth surface from a point cloud without the use of NURBS is an issue because refining the mesh will not change how smooth the mesh is. However, when generating a NURBS surface which in turn generates a series of B-splines a smooth and continuous surface can be generated with smoother interpolations.



## CHAPTER 3: AUTOMATED NURBS MESH GENERATOR

### 3.1 Introduction

Before initializing a computational simulation, the type of mesh should be carefully considered. The purpose of the mesh is to accurately represent the geometry that the simulation is being performed on. When describing a surface, there are two main types of element that are used: triangular and quadrilateral [21]. Each element type has its own advantages and disadvantages. However, it is still important to know that representing a highly curved surface with either element type requires a dense mesh since the curve is represented by a series of straight lines (or curved surface is represented by a series of triangular/quad planes). Alternatively, NURBS allows us to represent a surface using various lines instead of simple, straight lines. This allows us to reduce the mesh density while producing an accurate representation of the object geometry.

This chapter focuses on the algorithms used to develop the automated NURBS mesh generator. The NURBS mesh generator allows us to take in an ordered point cloud, and return a surface mesh with minimal user input.

### 3.2 Main Framework

The inputs required are the point cloud and an a text input file, which includes the number of points in the point cloud, the number of nodes in both parametric directions, the degree of NURBS that is desired, and whether or not it is an open or closed mesh. Using the specified inputs, the code generates a NURBS surface mesh.

The systematic approach used to generate the NURBS mesh can be seen in Figure 11 below. The first step, after reading in the information from the input file, is to assign values for the knot vectors, weight vectors, and mesh indices. Next, the initial mesh is generated using the read surface points as the initial position for control points. The steepest descent is an optimization method used to reduce the cost function. In this case, the function would represent the overall difference between the generated NURBS surface and the point cloud. When the convergence criteria is met, the final mesh generation is done. Finally, an Initial Graphics Exchange Specification (IGES) file is generated which is used to visually represent the final product.

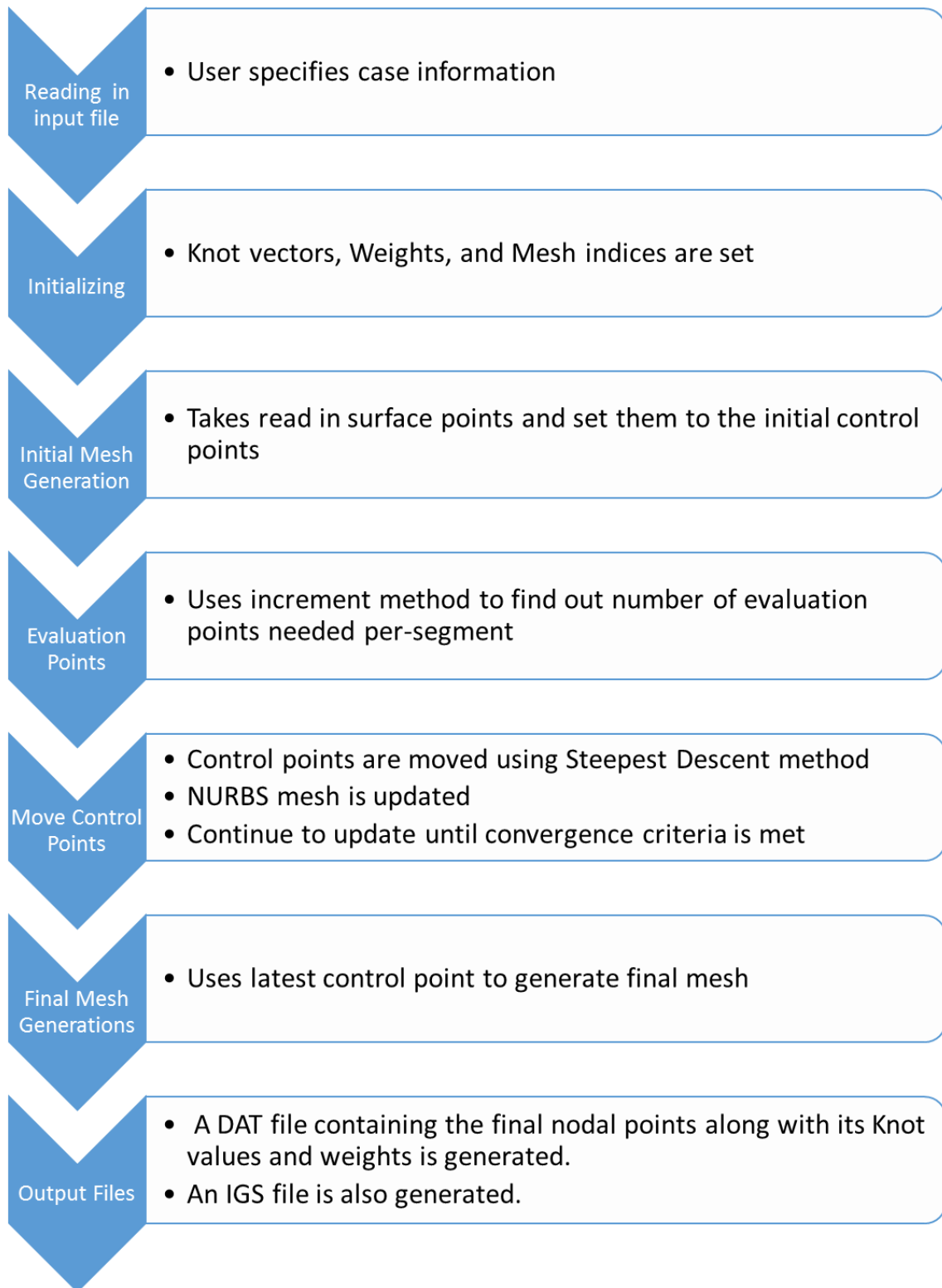


Figure 12: Overview flow of Automated NURBS Generator.

The NURBS generation algorithms, used to encapsulate the point cloud geometry, can be broken down to three main components: NURBS basis functions, surface smoothing, and moving control points.

### 3.2.1 NURBS Basis Functions

In order to generate the NURBS curve, some parameters need to be set. Initially the point cloud that is read in is initialized as the positions for the control points. After reading in the control points and the input file the domain is defined. The basis functions require a knot vector and weight values. To insure a smooth and continuous curve the knot vector that is to be used needs to be an increasing sequence. In the example of generating a 2<sup>nd</sup> degree NURBS curve with 9 control points the generated knot vector would be as follows:

$$U = (0,0,0,1,2,3,4,5,6,7,7,7)$$

After assigning the knot vector the generation process may begin. A single ‘patch’ is generated first. This patch uses the first 3 control points, which are initially the first 3 point cloud points. Following, the NURBS patch moves first along the U direction until it reaches the end, this can be seen for this example in the Figure 12 below.

$$\text{Surface points} = \begin{bmatrix} 1.0000 & 0.0000 \\ 0.7071 & 0.7071 \\ 0.0000 & 1.0000 \\ -0.7071 & 0.7071 \\ -1.0000 & 0.0000 \\ -0.7071 & -0.7071 \\ 0.0000 & -1.0000 \\ 0.7071 & -0.7071 \\ 1.0000 & 0.0000 \end{bmatrix}$$

Figure 13: The selection of the control points being selected to generate individual patches.

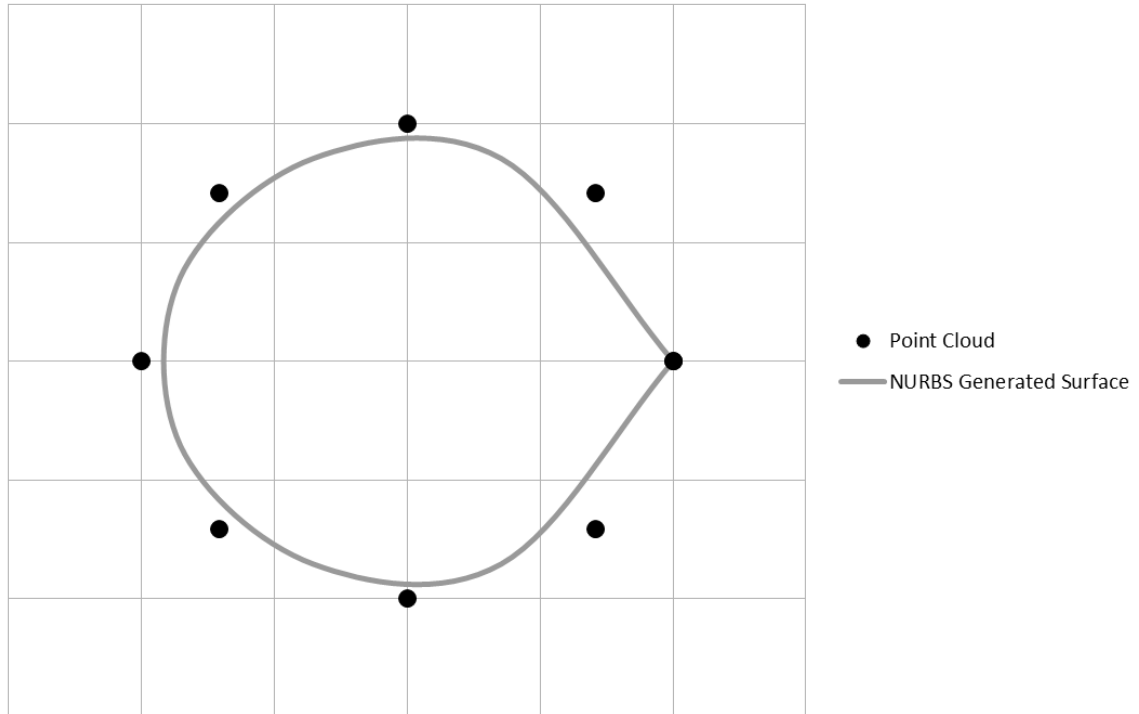


Figure 14: Initial generation of 1D NURBS curve before control points are moved.

Expanding the same concept to generate a 2D NURBS surface is not much different. However due to the fact that there are now two different parametric directions, two knot vectors need to be generated. Similarly to how the knot vector for the  $u$ -direction was generated another is generated for the  $v$ -direction.

Again in order to generate the NURBS surface, a single patch is generated this time with 3 control points along the  $u$ -direction by 3 control points along the  $v$ -direction. Following, the NURBS patch moves first along the  $U$  direction until it reaches the end. The patch then moves up a single node in the  $V$  direction, and goes through the  $U$  direction once more. The generation of a single patch is consisted of using the basis functions that are generated using the knot vector values along with the weights for that patch.

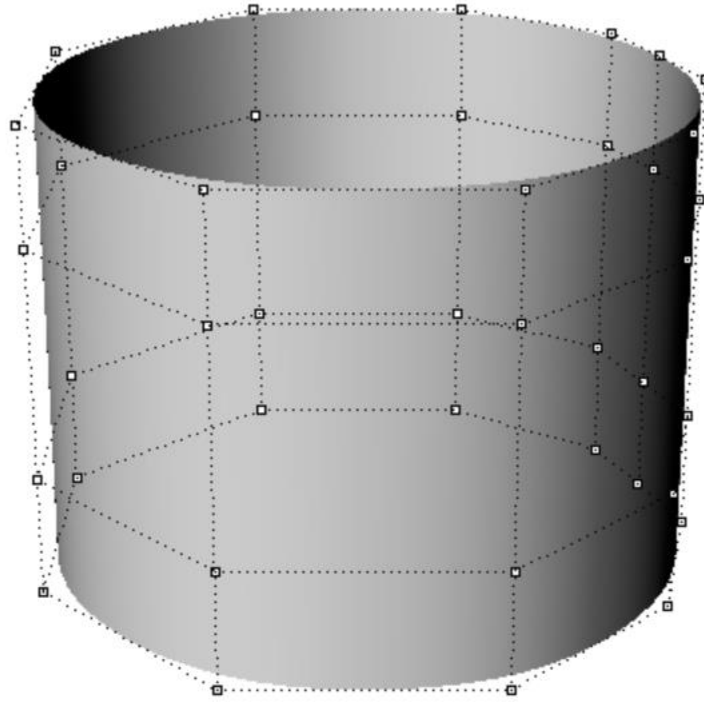


Figure 15: 2D NURBS surface generated.

When the final mesh is generated, IGES and DAT files are generated as outputs. The IGES file can be opened in Rhino to inspect mesh quality. The generated DAT file contains control point values, surface point values, the knot vectors, and the weight vectors for both parametric directions.

### 3.2.2 Surface Smoothing

To create a smoother seam, an additional, necessary step is used. With more sparse point clouds, the seam tends to be sharp and can be smoothed. This issue can be resolved by the user turning on the switch in the user input file. When this option is turned on, there

are two additional points that are added to each “ring”.

Using this method, the algorithm first searches and separates the point cloud into rings. After they have been separated into rings, the points that lay on the seam and their neighbors are also identified. Two interpolations are done one between the seam point and the leading neighbor and the other is between the seam and trailing neighbor. To assure a smoother curvature at the seam, the first radius is calculated between the seam point and the center of the ring. This is labeled in the example Figure 15 below as  $R_2$ . Similarly, the radii are calculated from the center to the leading point, and from the center point to the trailing points, named as  $R_1$  and  $R_3$  respectively. An average the magnitudes of the radius is calculated between  $|R_2|$  and  $|R_1|$  that will serve as the interpolation magnitude for the point between the seam and the leading point  $|R_{\text{leading}}|$ . The magnitude used for the interpolation for the point between the seam point and the trailing point,  $|R_{\text{trailing}}|$ , uses the average between  $|R_2|$  and  $|R_3|$ .

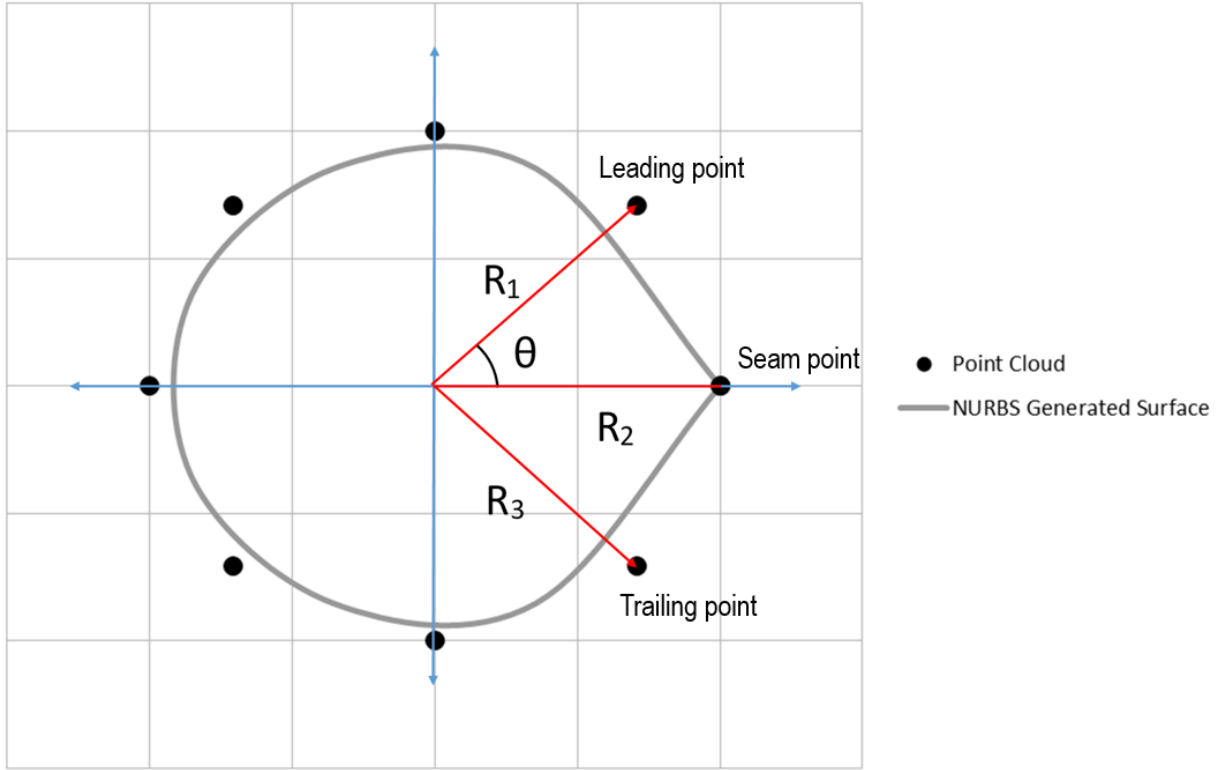


Figure 16: Selecting appropriate points for interpolation between the leading point and the seam and the trailing point and the seam for a 1 D case.

Following calculating the magnitudes for the leading and trailing supporting control points, the normal of the original vectors are calculated. Taking the average of the normalized  $R_2$  ( $\hat{r}_2$ ) and  $R_1$  ( $\hat{r}_1$ ) to get  $R^*_{leading}$ . Likewise with when trying to calculate  $R^*_{trailing}$ , the average of the normalized  $R_2$  ( $\hat{r}_2$ ) and  $R_3$  ( $\hat{r}_3$ ) is taken. However taking the average of two normalized vectors yields a vector that is no longer a unit vector, so the resulting vectors are normalized once more. The new resulting unit vectors  $\hat{r}_{leading}$  and  $\hat{r}_{trailing}$  will serve as our directional vectors. The final step in generating the two additional points would be to take the magnitude of both the leading and trailing averages and multiply it by the unit vector in the appropriate direction. The final result for the example shown in Figure 16 below.



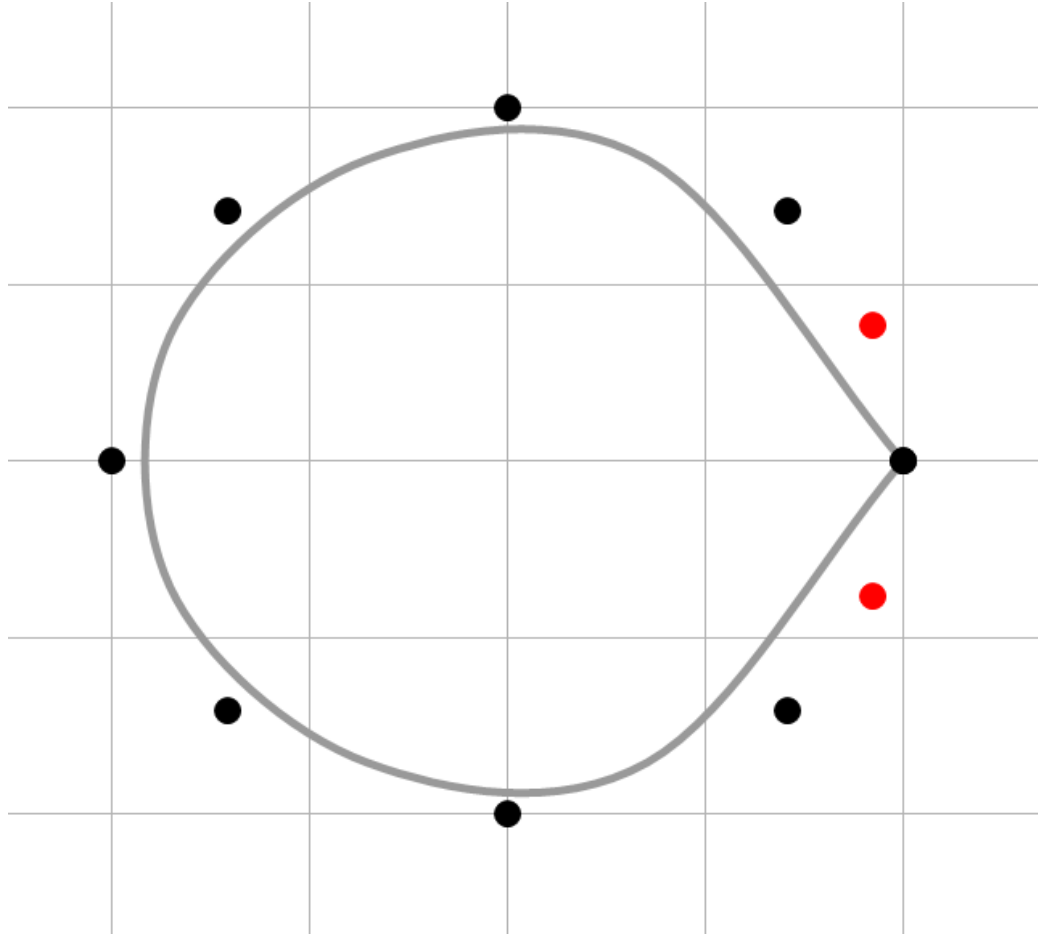


Figure 17: The addition of two new point cloud points can be seen in red.

### 3.2.3 Moving Control Points

Having the initial guess for the control points be the position of the point cloud points is an adequate starting point. After generating the initial mesh with the read in point cloud as the starting point. Moving these control points so the final geometry lands on the point cloud is what is seek to be archived. The steepest decent optimization method can be used to determine which direction to move the control points in order for the surface points to land on the desired position.

Before actually moving the control points being able to properly calculate how off the generated surface is to the ideal surface is crucial. When a NURBS surface is generated, it is generated based on mathematical expressions. The initial mesh was generated using a full knot spacing. However when the point cloud is sparse evaluating the surface at a full knot spacing might give a false distance. Reverting to the circle example where there were only 8 distinct surface points a portion of it can be seen in the Figure 17 below how a full knot spacing might be misleading.

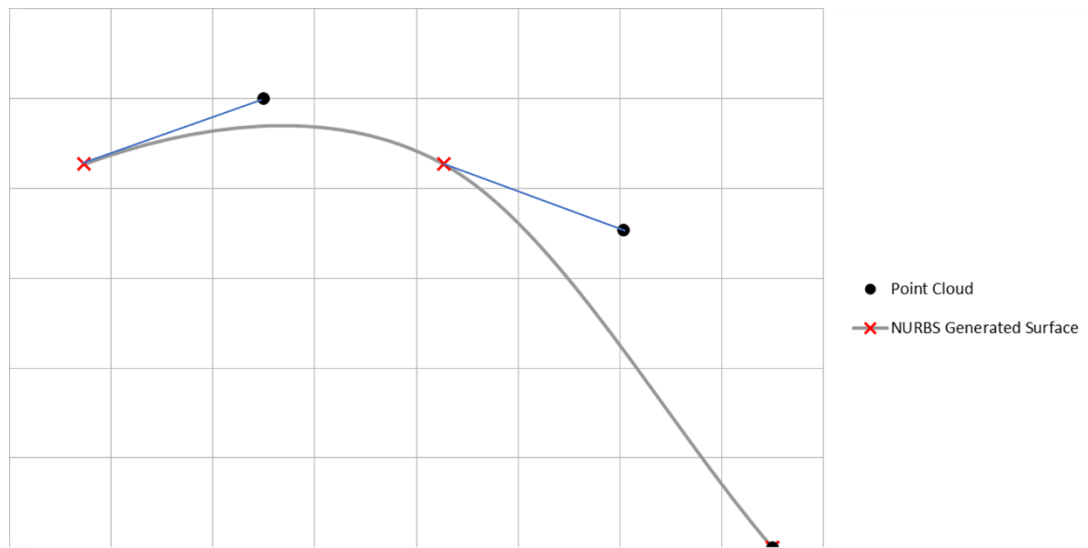


Figure 18: Initial evaluation points when marching a full knot spacing.

Therefore, the NURBS curve may need to analyze more frequently to assure higher accuracy. In doing so, an incremental process is done to find out how many times each segment needs to be evaluated. In this algorithm initially each segment is divided into two. Then the shortest distances are calculated between the point cloud and the generated surface using a nearest distance search algorithm. These distances are then compared to that of surface that was evaluated 3 times per segment. This iterative process continues

until there is less than a 5% change between the new number of evaluation and the previous iteration. Figure 18 below shows two segments split 10 times each. This approach estimated more accurate values closer to the desired positions.

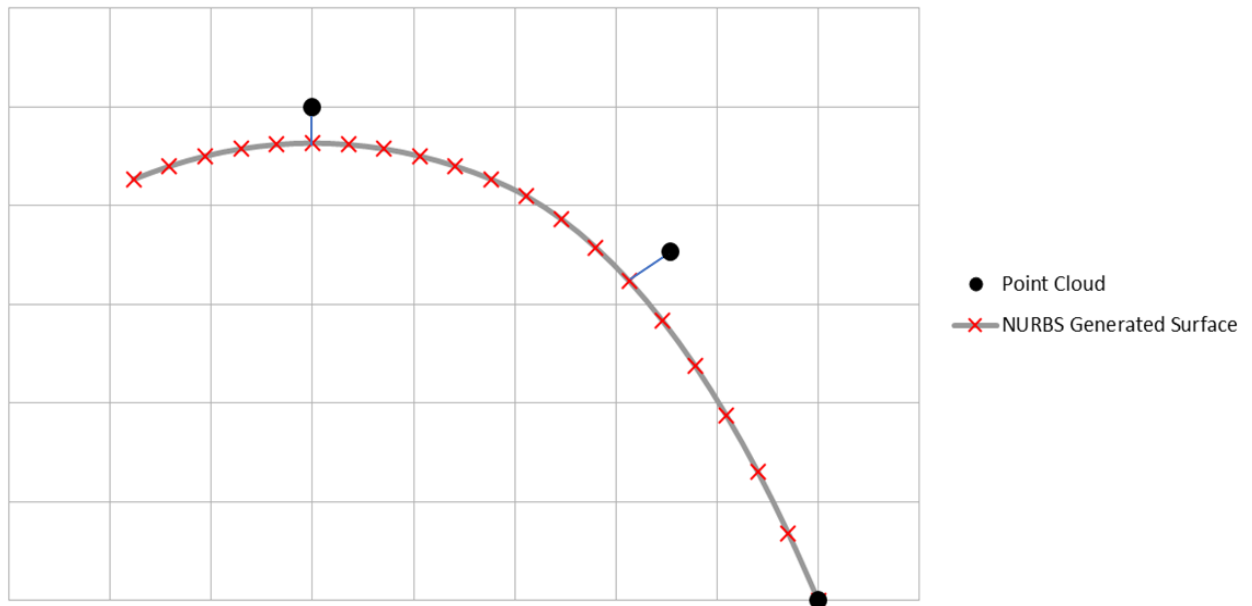


Figure 19: Ten evaluations are done per line segment and the closest surface point are detected.

### 3.3 Steepest Descent Algorithm

The next step is to move the nearest detected points to the location of the read surface points. The method used to assure the control points move in the right direction is an optimization method known as the steepest descent method. The steepest descent method uses an incremental process and a stopping criteria to insure a convergence of the design variables. The steepest descent algorithm does not have a limit on the number of variables used. An overview look at the iterative process is presented in Figure 19 below.

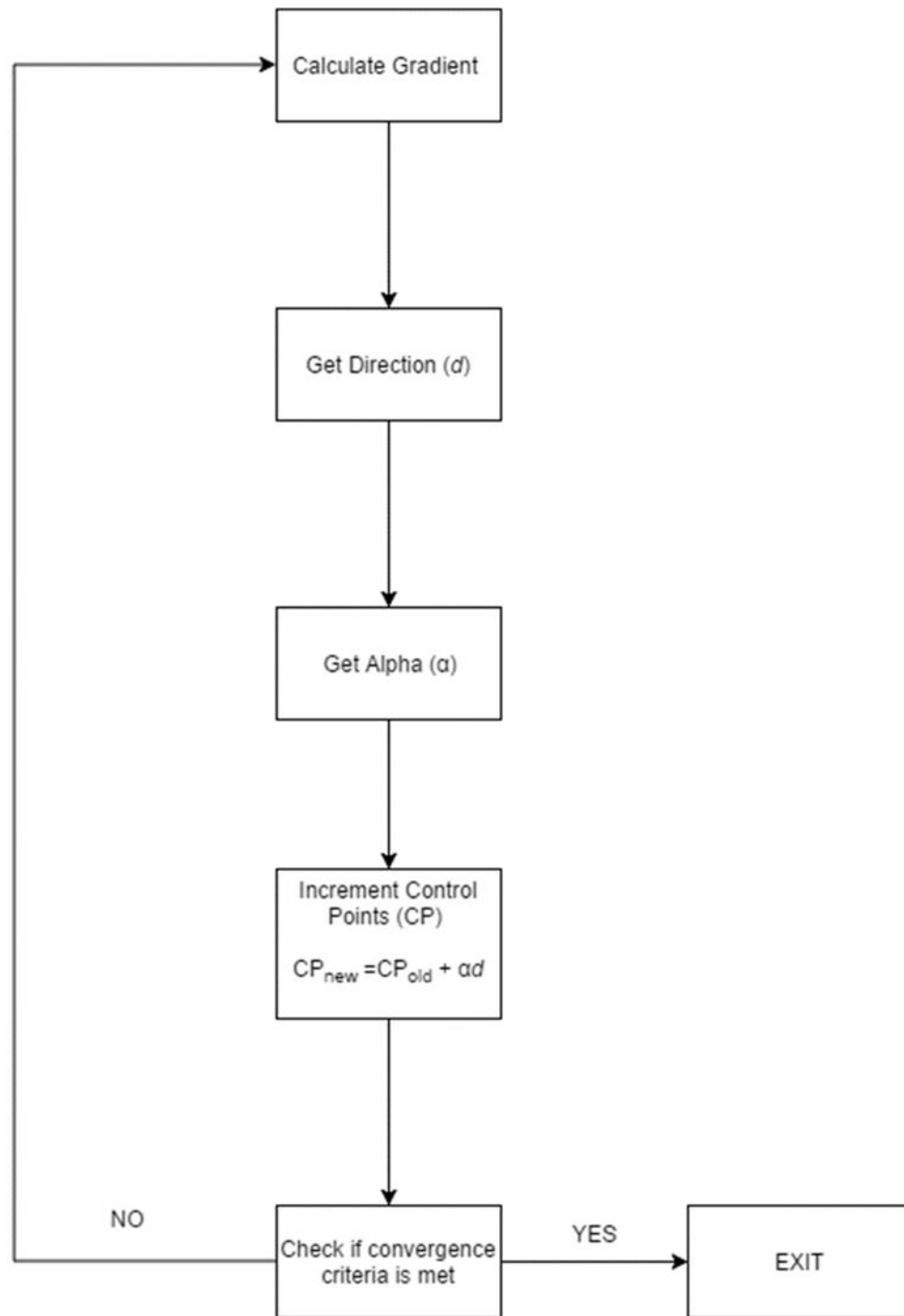


Figure 20: Flow chart representing iterative process of the Steepest Decent

The steepest descent method used is a one-dimensional method. This means there is a single parameter being optimized per design variable. Therefore, each point cloud in

the three-dimensional space is broken down into its X, Y, and Z components and set as individual design variables.

There is a set maximum number of iteration that this process may take this is set there will not be an incident where an infinite loop is created. After every iteration the summation of the norm of the gradient used in the cost function is calculated. This will serve as our stopping criteria. The default convergence criteria is set to be 0.005 in the work presented here. Before using the steepest descent algorithm, the input (i.e. “the initial guess”) needs to be known. A NURBS surface mesh is generated using the initial reading surface point as the initial position for the control points.

### 3.3.1 Cost Function

The steepest descent algorithm uses a function to minimize the output, known as the cost. The algorithm, or cost function, should be written in terms of the design variables. As mentioned in the above chapter the formulation of the NURBS surface can be seen in Equation below. The design variables that are being optimized here are the control points  $P_{i,j}$  in Equation 8.

$$S(u, v) = \frac{\sum_{i=0}^n \sum_{j=0}^m N_{i,p}(u) \cdot N_{j,q}(v) \cdot w_{i,j} \cdot P_{i,j}}{\sum_{i=0}^n \sum_{j=0}^m N_{i,p}(u) \cdot N_{j,q}(v) \cdot w_{i,j}} \quad \text{Equation 8}$$

Equation 9 below demonstrates how the control points and design variables are incorporated into the cost function.  $S_{ideal}$  represents the read surface points that we would like to have our final surface fit too. This cost function takes in consideration the entire geometry at once, where  $n$  represents the number of surface points in the data structure.

$$\text{cost function} = f = \frac{1}{2} \sum_{i=1}^n \left[ (S(u, v)_{\text{generated}})_i - (S_{\text{ideal}})_i \right]^2 \quad \text{Equation 9}$$

### 3.3.2 Gradient

The stopping criteria uses the norm of the pre-determined function gradient. The norm of the gradient is calculated at the end of every iteration to confirm if it has been met. Calculation of the gradient needs to be in terms of the design variables in the cost function. Having the control points,  $\mathbf{P}_{i,j}$ , be the design variables the formulation of the gradient can be seen in Equation 10 below:

$$\nabla f = \sum_{i=1}^n \left[ (S(u, v)_{\text{generated}})_i - (S_{\text{ideal}})_i \cdot S'(u, v)_{\text{generated}} \right] \quad \text{Equation 10}$$

$$S(u, v) = \frac{\sum_{i=0}^n \sum_{j=0}^m N_{i,p}(u) \cdot N_{j,q}(v) \cdot w_{i,j} \cdot \mathbf{P}_{i,j}}{\sum_{i=0}^n \sum_{j=0}^m N_{i,p}(u) \cdot N_{j,q}(v) \cdot w_{i,j}} = \sum_{i=0}^n \sum_{j=0}^m R_{i,j}(u, v) \cdot \mathbf{P}_{i,j}$$

The formulation shows  $S'(u, v)_{\text{generated}}$  which is the derivative of the NURBS formulation with respect to  $\mathbf{P}_{i,j}$ . Below the NURBS formulation can be rewritten as seen in the Equation above. Taking the derivative with respect to control points leaves us with the shape functions  $A_{i,a}$  in Equation 11 below.

$$S'(u, v) = \sum_{i=0}^n \sum_{j=0}^m A_{i,j} \cdot \mathbf{P}_{i,j} \quad \text{Equation 11}$$

### 3.3.3 Golden Section Method

Golden section method is a gradient based search algorithm that finds the minimum value of a one dimensional function. In order to do so, any multi-dimensional function should be converted into a one dimensional one. This is why it is called a line search algorithm that finds a minimum  $\alpha$  value. The parameter  $\alpha$  is the maximum step length that could be taken in a certain iteration in the algorithm [22]. This is required to reach the minimum value of the aforementioned one dimensional function. This is done at each single iteration within the steepest decent optimization algorithm. Equations 12, 13, and 14 are used in the steps shown below to calculated  $\alpha$

$$\alpha_q = \sum_{j=0}^q \delta(1.681)^j ; q = 0,1,2, \dots \quad \text{Equation 12}$$

$$f(\alpha_{q-1}) < f(\alpha_{q-2}) \text{ and } f(\alpha_{q-1}) < f(\alpha_q) \quad \text{Equation 13}$$

$$\alpha_u = \alpha_q = \sum_{j=0}^q \delta(1.681)^j ; \alpha_l = \alpha_{q-2} = \sum_{j=0}^{q-2} \delta(1.681)^j \quad \text{Equation 14}$$

Find  $\alpha$  to minimize  $f(\alpha)$ .

**Step 1-** *Phase I:* Initialize  $\delta$  to a small value (ex. 0.001), then calculate

$f(0), f(\alpha_0), f(\alpha_1), \dots$ , where  $\alpha_i$  are given by Equation 12. Let  $q$  be the smallest integer to satisfy Equation 13, where  $\alpha_q, \alpha_{q-1}$ , and  $\alpha_{q-2}$  are calculated from Equation 12. The upper and lower bounds ( $\alpha_l$  and  $\alpha_u$ ) on  $\alpha^*$  (optimum value for  $\alpha$ ) are given by Equation 14. The interval of uncertainty is given as  $I = \alpha_u - \alpha_l$ .

**Step 2-** *Phase II:* Compute  $f(\alpha_b)$ , where  $\alpha_b = \alpha_l + 0.618I$ . First iteration,

$$\alpha_a = \alpha_l + 0.382I = \alpha_{q-1} \text{ and so } f(\alpha_a) \text{ is already known.}$$

**Step 3-** Compare  $f(\alpha_a)$  and  $f(\alpha_b)$ , and go to (a), (b), or (c).

- a. If  $f(\alpha_a) < f(\alpha_b)$ , then minimum point  $\alpha^*$  lies between  $\alpha_l$  and  $\alpha_b$ , that is,  
 $\alpha_l \leq \alpha^* \leq \alpha_b$ . The new limits for the reduced interval of uncertainty are  $\alpha'_l = \alpha_l$  and  $\alpha'_u = \alpha_b$ . Also,  $\alpha'_b = \alpha_a$ . Compute  $f(\alpha'_a)$ , where  $\alpha'_a = \alpha'_l + 0.382(\alpha'_u - \alpha'_l)$  and go to Step 4.
- b. If  $f(\alpha_a) > f(\alpha_b)$ , then minimum point  $\alpha^*$  lies between  $\alpha_a$  and  $\alpha_u$ , that is,  
 $\alpha_a \leq \alpha^* \leq \alpha_u$ . Similar to the procedure in Step 3(a), let  $\alpha'_l = \alpha_a$  and  $\alpha'_u = \alpha_u$ , so that  $\alpha'_a = \alpha_b$ . Compute  $f(\alpha'_b)$ , where  $\alpha'_b = \alpha'_l + 0.618(\alpha'_u - \alpha'_l)$  and go to Step 4.
- c. If  $f(\alpha_a) = f(\alpha_b)$ , let  $\alpha_l = \alpha_a$  and  $\alpha_u = \alpha_b$  and return to Step 2.

If the new interval of uncertainty  $I' = \alpha'_u - \alpha'_l$  is small enough to satisfy a stopping criterion (i.e.,  $I' < \varepsilon$ ), let  $\alpha^* = (\alpha'_u + \alpha'_l)/2$  and stop. Otherwise, delete the primes on  $\alpha'_l, \alpha'_a$ , and  $\alpha'_b$  and return to Step 3[22]



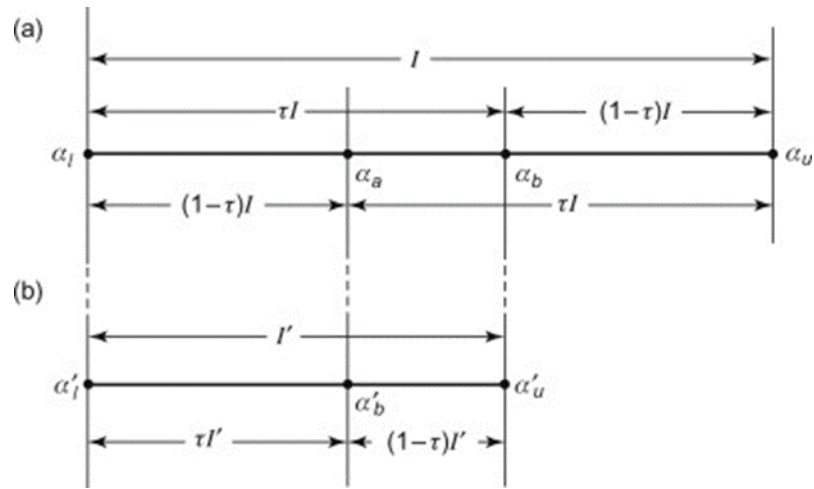


Figure 21: Golden section search representation.

The steepest decent method applies the constant,  $\alpha$ , to properly change the design variables. Equation 15, below, describes the iteration technique used to optimize and reach the convergence criteria of the steepest descent.

$$\bar{x}_{new} = \bar{x}_{old} + \alpha \bar{d} \quad \text{Equation 15}$$

## CHAPTER 4: RESULTS AND DISCUSSION

### 4.1 Introduction

To verify the automated NURBS mesh generator previously discussed, three different geometries were simulated and tested, including a cylinder, sphere and a cone. The geometries were resembled using ordered point cloud files. In addition, two different patient-specific mitral valves and three coronary arteries were also generated. These patient-specific geometries were used to demonstrate the capability of the NURBS generator.

### 4.2 Analytical Geometries

#### 4.2.1 Cylinder

The cylinder input file includes four circular rings with a radius of 1, centered at the origin on the X-Y plane. The generated point cloud for the cylinder contains a total of 36 points - 9 in the radial direction forming a slice, and 4 slices along the Z direction. Figure 21 below is a visual representation of the point cloud.



Figure 22: Generated cylindrical point cloud that is centered on the z-axis with a radius of 1 and a height of 2.

A NURBS surface was generated using a point cloud file and a specification file. A specification file includes total number of control points, number of nodes in each parametric direction, the degree of the generated NURBS surface, and whether it is an opened/closed (i.e. end-to-end) surface. The NURBS surface was then optimized to fit the point cloud within the tolerance limit, as seen in Figure 22 below.

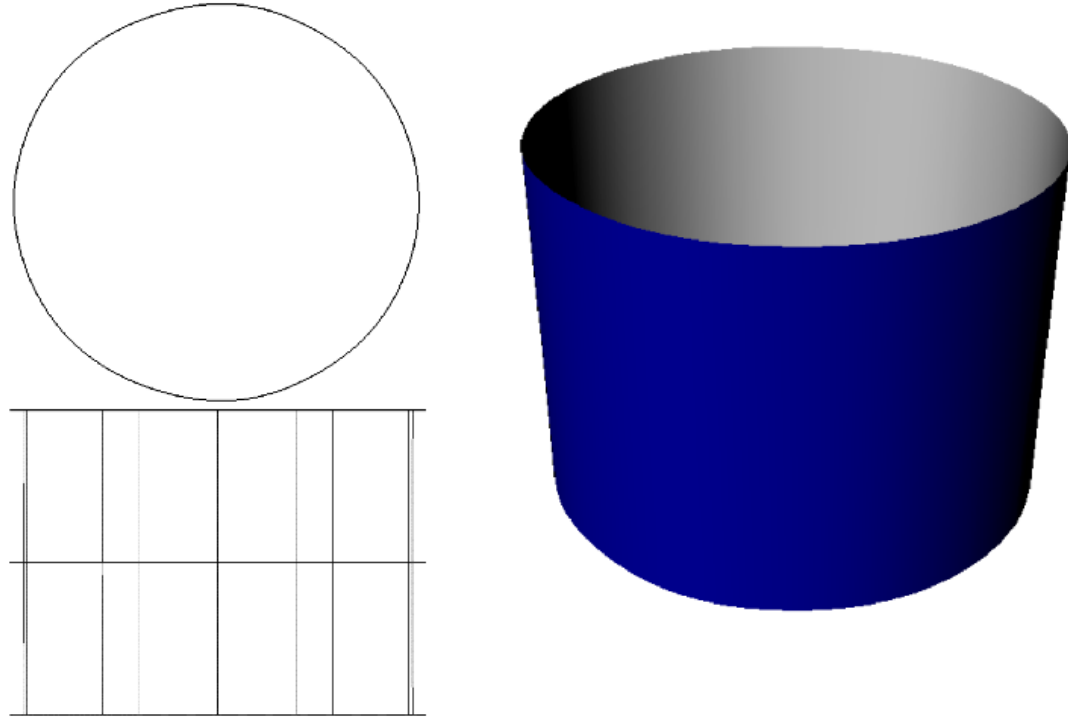


Figure 23: Optimized NURBS generation of Cylindrical Point cloud.

#### 4.2.2 Cone

The generated cone had a base radius of 1 and a height of 5. The generated surface points included 17 points in the X-Y plane forming a slice and 26 slices in the Z-direction this can be seen in Figure 23 below.

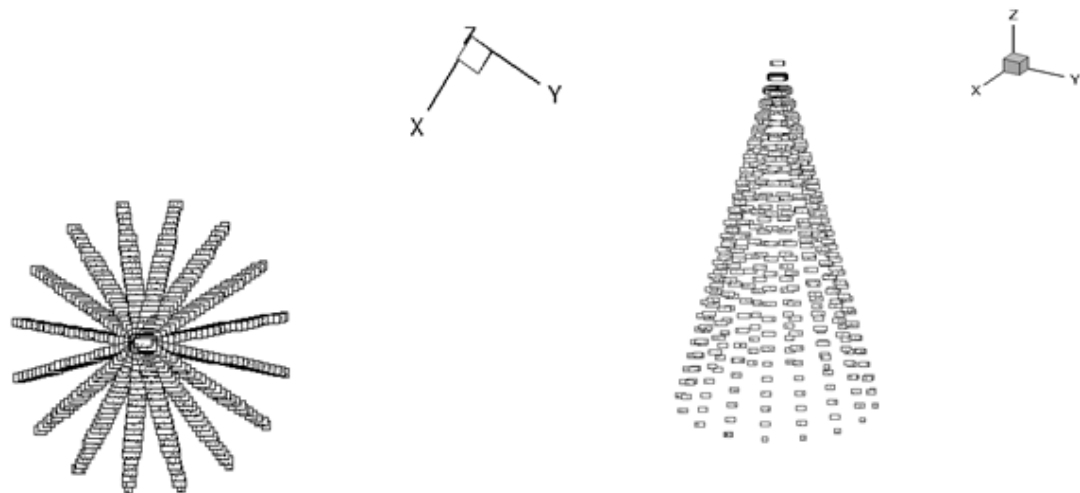


Figure 24: Generated Cone point cloud

A NURBS surface was generated using a point cloud file and a specification file. The NURBS surface was then optimized to fit the point cloud within the tolerance limit, as seen in Figure 24 below.

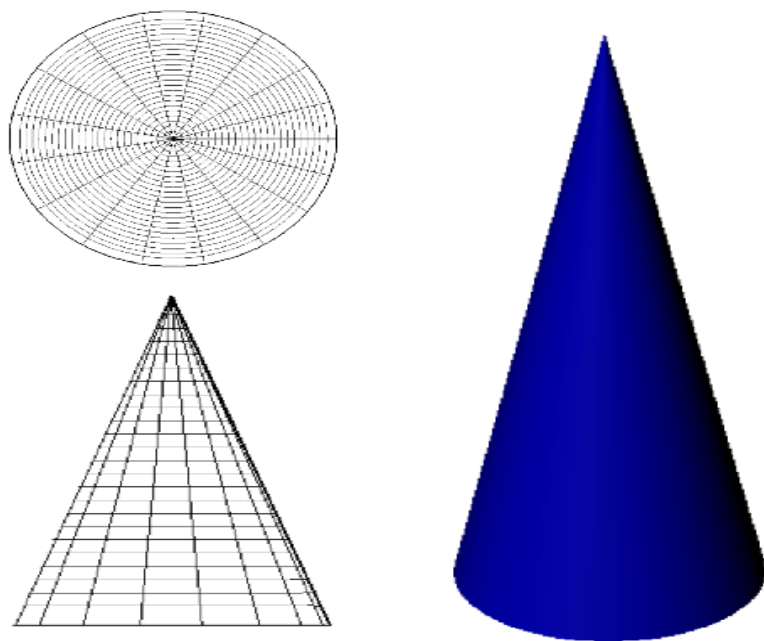


Figure 25: Optimized NURBS surface generated by cone point cloud

### 4.2.3 Sphere

The point cloud for a sphere was generated while centering it along the X-Y plane. The radius of the generated sphere was 1. The point cloud included 153 points - 17 points in the radial direction forming a slice and 9 slices were generated in the Z-direction as seen in Figure 25 below

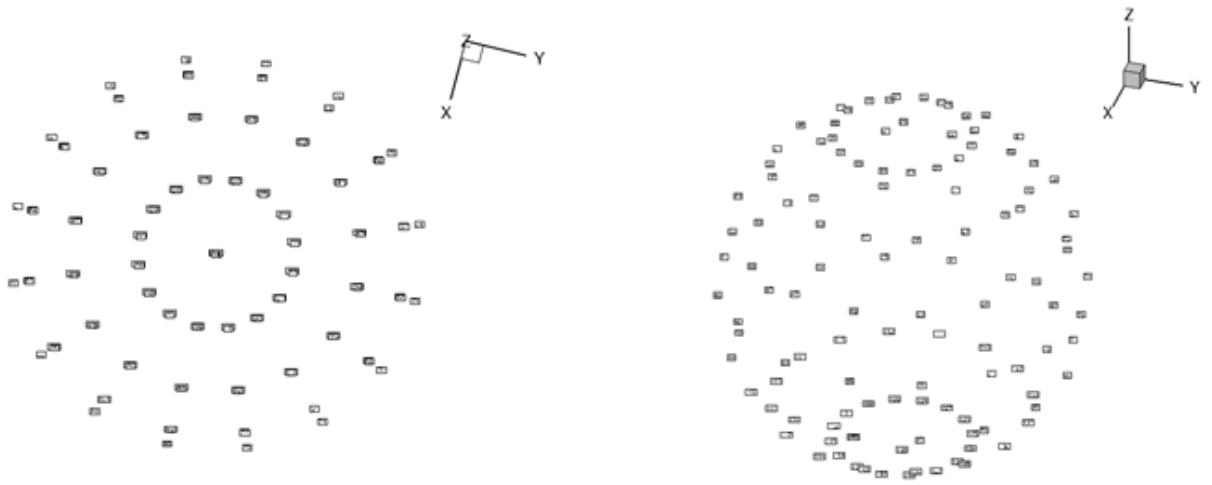


Figure 26: Generated Spherical point cloud with a radius 1.

A NURBS surface was generated using a point cloud file and a specification file. The NURBS surface was then optimized to fit the point cloud within the tolerance limit, as seen in Figure 26 below.

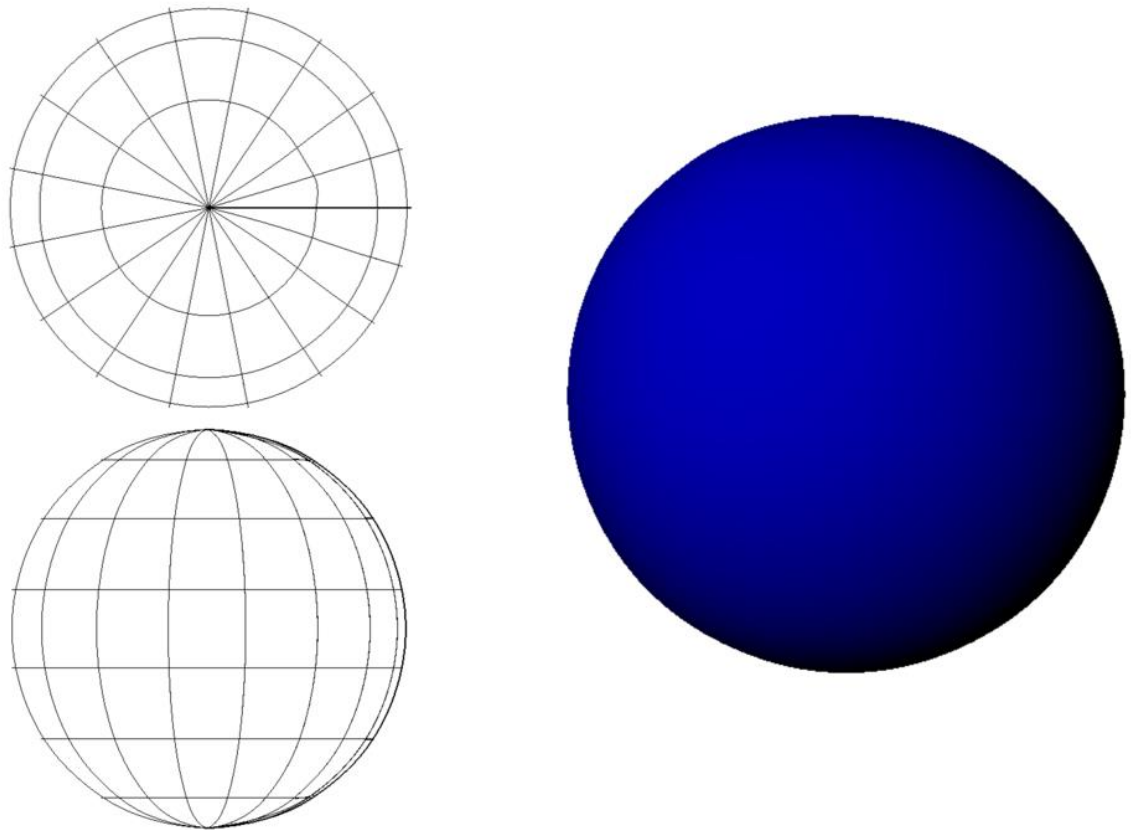


Figure 27: Optimized NURBS surface generated from spherical point cloud

After simulating these geometries from their respective point clouds, a survey of points were collected from the generated surfaces. The points that were selected to compare were found by using the ‘nearest point’ search algorithm. Differences between the generated surface and the point cloud points were then calculated, in terms of percent error. This was used as an overall summary measure to validate the NURBS generator. Figure 27 and Table 1 below shows the percent errors plotted for each geometry.

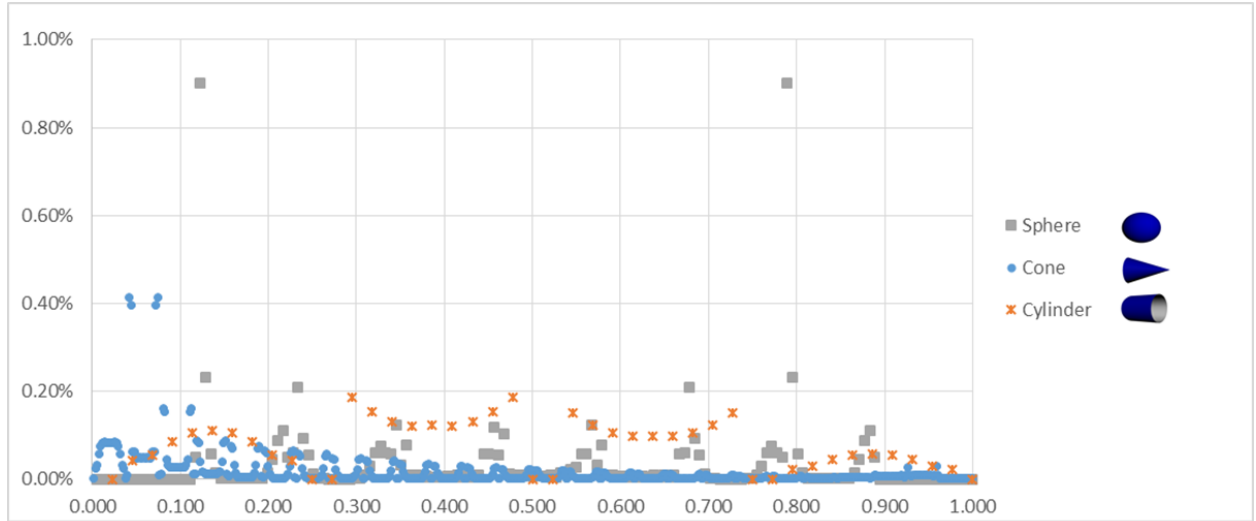


Figure 28: Scattered plot of percent error between NURBS generated surface and analytical solutions for: Sphere, Cone and Cylinder.

Shape	RMS Value	Max % Error	Average % Error	Standard Deviation ( of % Error)
Cone	0.000491315	0.41%	0.02%	0.0422038
Cylinder	0.001844958	0.19%	0.08%	0.0555325
Sphere	0.001090780	0.90%	0.03%	0.1037640

Table 1: RMS values for percent error for all three analytical shapes.

The results demonstrate a low percent error among the three geometries. With the average error ranging from 0.02% - 0.08%, it can be seen the NURBS-generated surfaces accurately represent the actual geometries.



### 4.3 Patient Specific Point clouds

After validating the automated NURBS generator a set of patient-specific point clouds were used to generate NURBS based surfaces. These surfaces represent are what can be used to further study patient specific anomalies. Two different sets of biological measured point clouds where tested to show flexibility of the NURBS generator.

#### 4.3.1 Patient-Specific Mitral valve Point clouds

The mitral valve point clouds are an ordered point cloud that are consist of 37 points along the radial direction, to form a slice. There are 10 slices in each mitral valve. The point clouds for these patient specific mitral valve were taken using a Three-Dimensional Transesophageal Echocardiography.

### Patient 1 Mitral Valve

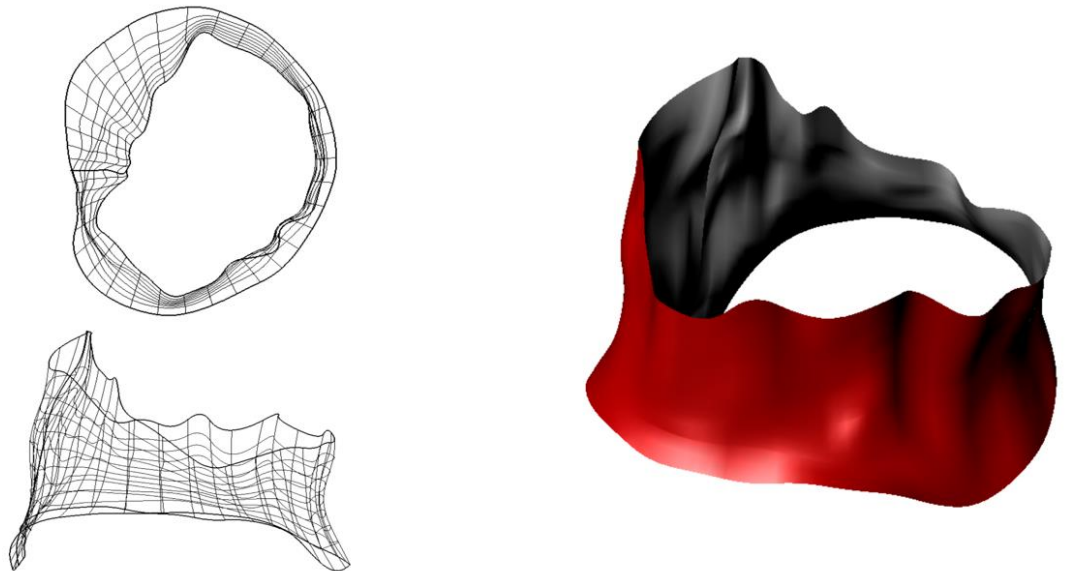


Figure 29: Optimized NURBS surface of Patient 1 mitral valve from point cloud.

## Patient 2 Mitral Valve

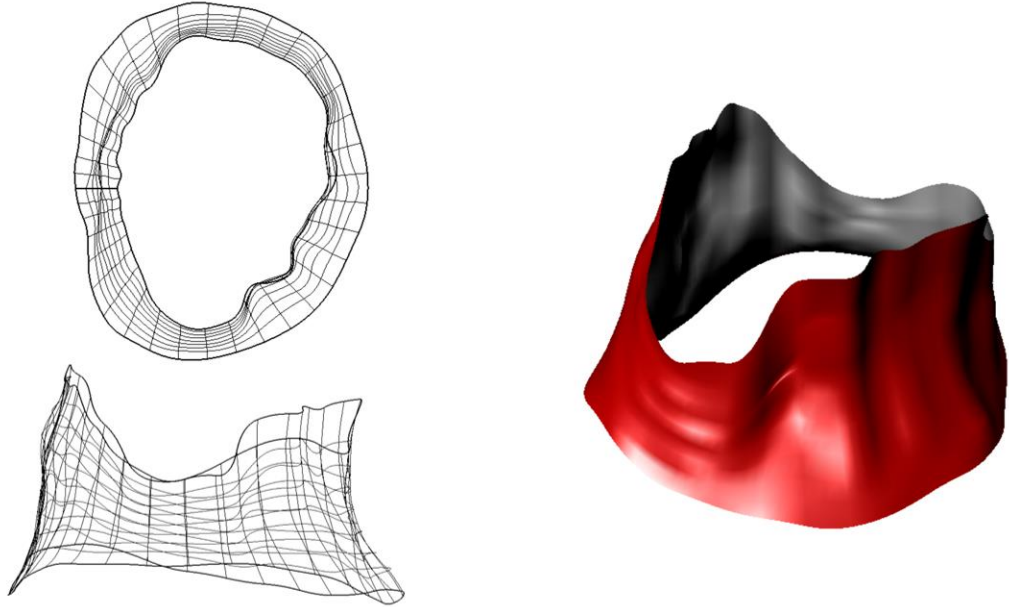


Figure 30: Optimized NURBS surface of Patient 2 mitral valve from point cloud.

### 4.3.2 Patient-Specific Coronary Artery Point clouds

The patient specific coronary artery point clouds were formed using angiography to capture the curvature and intravascular ultra sound to be able to capture the cross sections. These three patient specific point clouds contained 37 point along the radial direction. The number of slices differed from each patient. Table 2 below shows the number of sampled point in each direction for each patient.

	<b>Radial points</b>	<b>Number of slices</b>	<b>Total Number of Points</b>
<b>Patient 1</b>	37	127	4699
<b>Patient 2</b>	37	142	5254
<b>Patient 2</b>	37	107	3959

Table 2: Patient specific coronary artery point cloud specifications.

## Patient 1 Coronary Artery

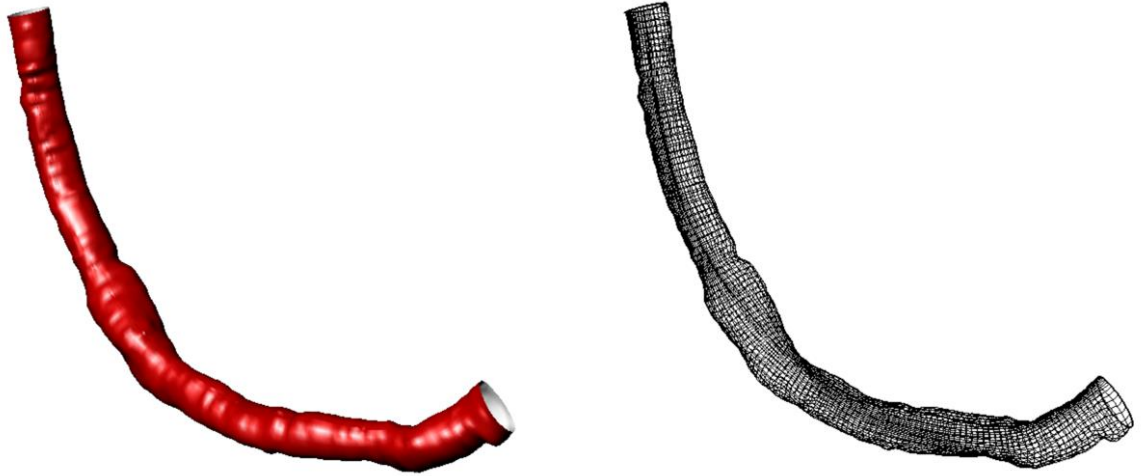


Figure 31: Optimized NURBS surface of Patient 1 coronary artery from point cloud.

## Patient 2 Coronary Artery

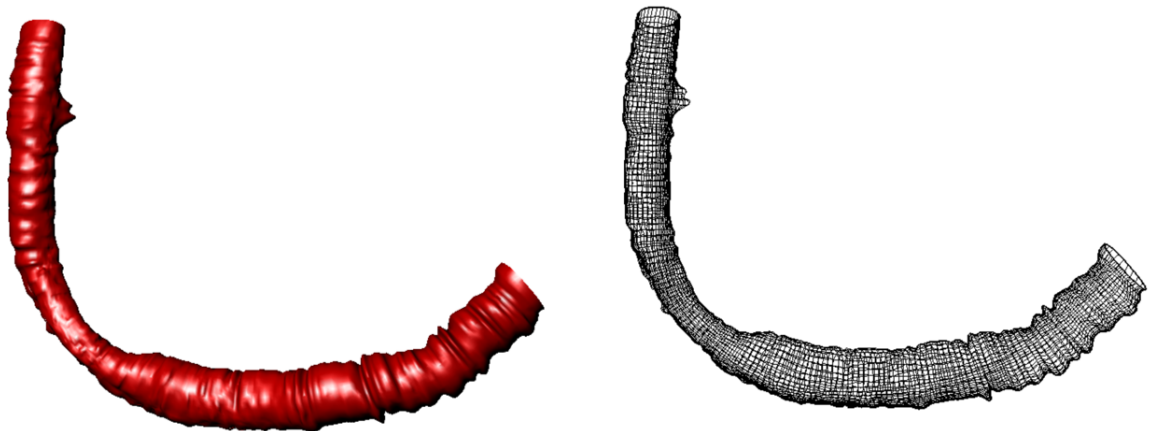


Figure 32: Optimized NURBS surface of Patient 2 coronary artery from point cloud.

## Patient 3 Coronary Artery

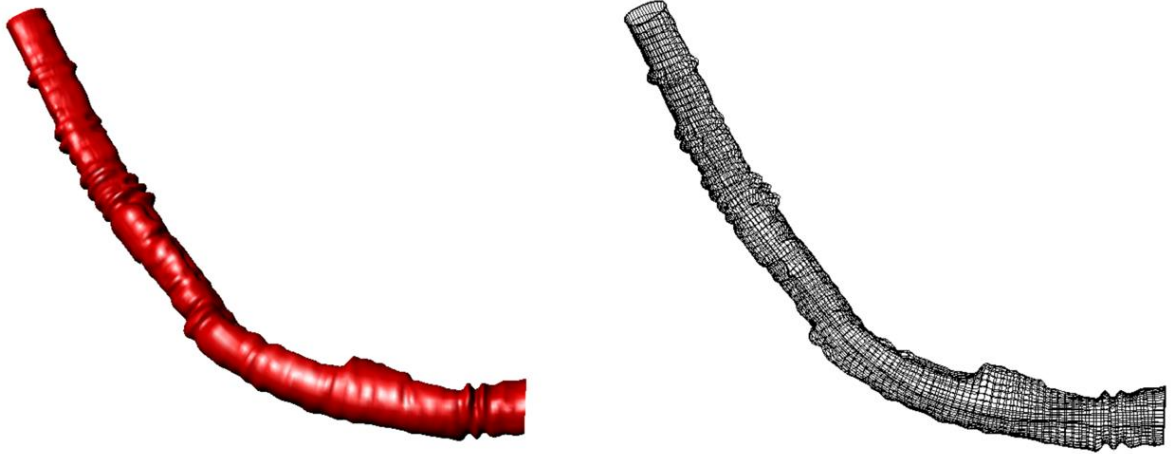


Figure 33: Optimized NURBS surface of Patient 3 coronary artery from point cloud.

### 4.4 Future Work

The current NURBS generator presented here has a few limitations that can be worked on. One of these limitations is that it requires a set of ordered points. Having such constrictions is not ideal. Moving forward being able to take in any set of points and fit a NURBS surface is the desired path. Also finding a way to minimize the number of control points being used would also be of interest to reduce computational cost.

### 4.5 Summary

When setting up computational simulations using cardiovascular tissue it is necessary to have smooth surfaces. With current methods of mesh generation the solution has been to increase the mesh density. The results of this study demonstrate that the NURBS generator is more capable of using patient-specific point clouds than traditional

methods. Using a NURBS surface to represent biological tissue removes the need to increase mesh densities just to avoid sharp edges. These results can be used to advance the medical knowledge regarding the complications of cardiovascular diseases.

## REFERENCES

- [1] W. G. Members, V. L. Roger, A. S. Go, D. M. Lloyd-Jones, E. J. Benjamin, J. D. Berry, W. B. Borden, D. M. Bravata, S. Dai, E. S. Ford, C. S. Fox, H. J. Fullerton, C. Gillespie, S. M. Hailpern, J. A. Heit, V. J. Howard, B. M. Kissela, S. J. Kittner, D. T. Lackland, J. H. Lichtman, L. D. Lisabeth, D. M. Makuc, G. M. Marcus, A. Marelli, D. B. Matchar, C. S. Moy, D. Mozaffarian, M. E. Mussolino, G. Nichol, N. P. Paynter, E. Z. Soliman, P. D. Sorlie, N. Sotoodehnia, T. N. Turan, S. S. Virani, N. D. Wong, D. Woo, and M. B. Turner, "Heart Disease and Stroke Statistics—2012 Update: A Report From the American Heart Association," *Circulation*, vol. 125, no. 1, p. e2, Jan. 2012.
- [2] P. C. McDonald, J. E. Wilson, S. McNeill, M. Gao, J. J. Spinelli, F. Rosenberg, H. Wiebe, and B. M. McManus, "The challenge of defining normality for human mitral and aortic valves: Geometrical and compositional analysis," *Cardiovasc. Pathol.*, vol. 11, no. 4, pp. 193–209, Jul. 2002.
- [3] E. J. Bekkers and C. A. Taylor, "Multiscale Vascular Surface Model Generation From Medical Imaging Data Using Hierarchical Features," *IEEE Trans. Med. Imaging*, vol. 27, no. 3, pp. 331–341, Mar. 2008.
- [4] C. J. Egelhoff, R. S. Budwig, D. F. Elger, T. A. Khraishi, and K. H. Johansen, "Model studies of the flow in abdominal aortic aneurysms during resting and exercise conditions," *J. Biomech.*, vol. 32, no. 12, pp. 1319–1329, Dec. 1999.
- [5] C. A. Taylor and C. A. Figueroa, "Patient-specific Modeling of Cardiovascular Mechanics," *Annu. Rev. Biomed. Eng.*, vol. 11, p. 109, 2009.
- [6] M. S. Sacks and A. P. Yoganathan, "Heart valve function: a biomechanical perspective," *Philos. Trans. R. Soc. B Biol. Sci.*, vol. 362, no. 1484, p. 1369, Aug. 2007.
- [7] "Bicuspid Aortic Valve | Congenital Heart Defects UK." .
- [8] J. Dreyfus, G. Durand-Viel, R. Raffoul, S. Alkhoder, U. Hvass, C. Radu, N. Al-Attar, W. Ghodbhane, D. Attias, P. Nataf, A. Vahanian, and D. Messika-Zeitoun, "Comparison of 2-Dimensional, 3-Dimensional, and Surgical Measurements of the Tricuspid Annulus Size Clinical Implications," *Circ. Cardiovasc. Imaging*, vol. 8, no. 7, p. e003241, Jul. 2015.
- [9] J. De Hart, G. W. M. Peters, P. J. G. Schreurs, and F. P. T. Baaijens, "A two-dimensional fluid–structure interaction model of the aortic valve," *J. Biomech.*, vol. 33, no. 9, pp. 1079–1088, Sep. 2000.
- [10] M. E. Silverman and J. W. Hurst, "The mitral complex: Interaction of the anatomy, physiology, and pathology of the mitral annulus, mitral valve leaflets, chordae tendineae, and papillary muscles," *Am. Heart J.*, vol. 76, no. 3, pp. 399–418, Sep. 1968.
- [11] H. Kim, J. Lu, M. S. Sacks, and K. B. Chandran, "Dynamic Simulation of Bioprosthetic Heart Valves Using a Stress Resultant Shell Model," *Ann. Biomed. Eng.*, vol. 36, no. 2, pp. 262–275, Nov. 2007.
- [12] C. A. Conti, A. Della Corte, E. Votta, L. Del Viscovo, C. Bancone, L. S. De Santo, and A. Redaelli, "Biomechanical implications of the congenital bicuspid aortic valve: A finite element study of aortic root function from in vivo data," *J. Thorac. Cardiovasc. Surg.*, vol. 140, no. 4, pp. 890–896.e2, Oct. 2010.
- [13] D. M. Dudzinski and J. Hung, "Echocardiographic assessment of ischemic mitral regurgitation," *Cardiovasc. Ultrasound*, vol. 12, no. 1, p. 46, Nov. 2014.
- [14] P. N. Jermihov, L. Jia, M. S. Sacks, R. C. Gorman, J. H. G. Iii, and K. B. Chandran, "Effect of Geometry on the Leaflet Stresses in Simulated Models of Congenital Bicuspid Aortic Valves," *Cardiovasc. Eng. Technol.*, vol. 2, no. 1, pp. 48–56, Jan. 2011.

- [15] A. M. Gillinov and D. M. Cosgrove, "Mitral Valve Repair," *Oper. Tech. Thorac. Cardiovasc. Surg.*, vol. 3, no. 2, pp. 95–108, May 1998.
- [16] A. Kiang-ia and S. Chatpun, "Mechanical analysis of mechanical aortic heart valve: Trileaflet versus bileaflet," presented at the Biomedical Engineering International Conference (BMEiCON), 2013 6th, 2013, pp. 1–4.
- [17] L. P. Dasi, H. A. Simon, P. Sucusky, and A. P. Yoganathan, "FLUID MECHANICS OF ARTIFICIAL HEART VALVES," *Clin. Exp. Pharmacol. Physiol.*, vol. 36, no. 2, p. 225, Feb. 2009.
- [18] J. De Hart, G. W. M. Peters, P. J. G. Schreurs, and F. P. T. Baaijens, "A three-dimensional computational analysis of fluid–structure interaction in the aortic valve," *J. Biomech.*, vol. 36, no. 1, pp. 103–112, Jan. 2003.
- [19] L. Piegl and W. Tiller, *The NURBS Book*, 2nd ed. .
- [20] S.-M. Hu, Y.-F. Li, T. Ju, and X. Zhu, "Modifying the shape of NURBS surfaces with geometric constraints," *Comput.-Aided Des.*, vol. 33, no. 12, pp. 903–912, Oct. 2001.
- [21] M. Viceconti, L. Bellingeri, L. Cristofolini, and A. Toni, "A comparative study on different methods of automatic mesh generation of human femurs," *Med. Eng. Phys.*, vol. 20, no. 1, pp. 1–10, Apr. 1998.
- [22] J. Arora, *Introductuion to Optimum Design*, 3rd ed. Elsevier Inc., 2012.